

## An experimental and theoretical approach of spectroscopic and structural properties of the bis(diethyldithiocarbamate)–cobalt(II)

A.C. Costa Júnior<sup>a,b</sup>, O. Versiane<sup>b</sup>, G. Faget Ondar<sup>b</sup>, J.M. Ramos<sup>c</sup>, Glaucio B. Ferreira<sup>a</sup>, A.A. Martin<sup>d</sup>, C.A. Téllez Soto<sup>a,d,\*</sup>

<sup>a</sup> Departamento de Química Inorgânica, Instituto de Química, Universidade Federal Fluminense (UFF), Morro do Valonguinho s/n, Niterói-Centro CEP 24210-150, RJ, Brazil

<sup>b</sup> Instituto Federal de Educação, Ciência e Tecnologia do Rio de Janeiro (IFRJ), Unidade de Rio de Janeiro, Rio de Janeiro, RJ, Brazil

<sup>c</sup> Instituto de Química, Universidade Federal do Rio de Janeiro, CP 68563, 21945-970 Rio de Janeiro, RJ, Brazil

<sup>d</sup> Laboratory of Biomedical Vibrational Spectroscopy, IP&D, Research and Development Institute – UNIVAP, Av. Shishima Hifumi, 2911 Urbanova, 12.224-000, São José dos Campos, SP, Brazil

### HIGHLIGHTS

- ▶ Synthesis of bis-diethyldithiocarbamate Co (II) was carried out.
- ▶ The FT-IR and Raman spectra of [Co(DDTC)<sub>2</sub>] were carried out.
- ▶ The Bond Orbital Analysis was used with the DFT method.
- ▶ The solid/solution UV–Vis spectra of [Co(DDTC)<sub>2</sub>] was measured.
- ▶ The calculated UV–Vis spectrum was performed using TD/PBE1PBE and TD/B3LYP methods.

### ARTICLE INFO

#### Article history:

Received 18 April 2012

Received in revised form 19 June 2012

Accepted 19 June 2012

Available online 26 June 2012

#### Keywords:

Bis(diethyldithiocarbamate)cobalt(II) complex

FT-infrared spectrum

DFT method

NBO analysis

UV–Vis spectrum

### ABSTRACT

Theoretical and experimental bands have been assigned for the Fourier Transform Infrared spectrum (FT-IR) and FT-Raman of the bis(diethyldithiocarbamate)Co(II) complex, [Co(DDTC)<sub>2</sub>]. The calculations have been based on the DFT/B3LYP method, second derivative spectrum and band deconvolution analysis. The UV–Vis experimental spectra of [Co(DDTC)<sub>2</sub>] was measured in the solid state and in an acetonitrile solution. The calculated electronic spectrum was estimated using the TD/PBE1PBE and TD/B3LYP methods 6-311G (d,p) basis set for all atoms.

The Bond Orbital Analysis was carried out with the DFT:B3LYP/PBE1PBE methods, revealing electronic delocalization effects involving Co–S and C=N bonds and their neighboring groups. The observed valence configurations for the alpha and beta electrons of the cobalt atom were (4s)<sup>0.46</sup>(3d)<sup>7.69</sup> (B3LYP) and (4s)<sup>0.46</sup>(3d)<sup>7.68</sup> (PBE1PBE), as expected for the planar structure around the Co(II) cation. The calculated infrared and UV–Vis spectra, based on the proposed geometrical structure of the bis(diethyldithiocarbamate)cobalt(II) complex, showed an excellent agreement with the experimental spectra.

Published by Elsevier B.V.

### 1. Introduction

The diethyldithiocarbamate ligand, known as DDTC [(ethyl)<sub>2</sub>NCS<sub>2</sub>], has been extensively studied in different fields, including industrial applications such as vulcanization additives, stabilizers for PVC, and also biological systems like fungicides, antibactericides and anti-cancer agent [1–4]. Dithio ligands are considered as soft donors, showing excellent coordination ability. They form

stable complexes with transition and non-transition metal ions and exhibit a variety of coordination modes both in homo and heteronuclear complexes [5,6]. An practical example of these properties is the association of some compounds containing dithio ligands with cisplatin. Berry et al. [7] carried out studies motivated by the chemoprotective action of these ligands, that allows doses up to 160 mg/m<sup>2</sup> of the drug, reducing the ototoxicity by inhibition of the nephrotoxic effects of cisplatin [3].

A better understanding of structure–property correlations for dithiocarbamates required several spectroscopic studies [8–10]. Bauer et al. [11] carried out a vibrational assignment of DDTC complex with zinc, cadmium and lead, but did not consider the coupling of the metal–sulfur stretching modes. Also, the investigation

\* Corresponding author at: Departamento de Química Inorgânica, Instituto de Química, Universidade Federal Fluminense (UFF), Morro do Valonguinho s/n, Niterói-Centro CEP 24210-150, RJ, Brazil.

E-mail address: [tellez@vm.uff.br](mailto:tellez@vm.uff.br) (C.A. Téllez Soto).

of the mixed toluene-3,4-dithiolatodialkyldithiocarbamates of arsenic(III) and bismuth(III), such as  $[C_6H_3(CH_3)_2MS_2CNR_2]$  ( $M=As$  and  $Bi$ ;  $R=CH_3$ ,  $C_2H_5$  and  $CH_2-CH_2$ ), was carried out by Chauhan et al. [12]. In this work, the infrared spectra present bands at 310–320 and 340–360  $cm^{-1}$ , assigned as  $As-S$  and  $Bi-S$  stretching vibrations, respectively. However, the assignment of pure metal-sulfur modes, existent in  $As$  and  $Bi$  complexes, is not observed in complexes forming rings of four or five members. In fact, a large number of studies not present conclusive assignments [10,13]. For example, San Andres et al. describe the spectrophotometric determination of copper(II), nickel(II) and cobalt(II) with diethyldithiocarbamate complexes without any detailed assignment of electronic bands [14]. Also, Mikosh et al. [15] reports a study of normal coordinate analysis in vibrational spectra for copper and nickel dithiocarbamate complexes, but the assignment in the region of the metal-ligand framework was not carried out. Some theoretical studies were also performed to understand different properties of dimethyl- and diethyldithiocarbamate complexes of  $Ag(I)$ ,  $Ni(II)$ ,  $Cu(II)$  and  $Zn(II)$  [13]. The calculations were based on density functional theory (DFT)/B3LYP and suggested that the important vibrational characteristic could be used to discern uni- and bidentate bonding through the Raman activity of the  $C-S$  stretching. No vibrational assignment of the framework vibrational region was done.

Although the  $[Co(DDTC)_2]$  complex belongs to a very important class of coordination compounds any conclusive structural, vibrational and electronic study were carried out. Due to this lack of information, we propose for this complex a synthesis route analysis, based on graphical method, and also complete spectroscopy study. The structural studies of the solid powder were carried out by means of FT-IR and Raman vibrational spectra and quantum mechanical theoretical calculations. The natural Bond Orbital Analysis (NBO) was also used with the purpose to study the charge transference properties in the complex. UV-Vis spectra were measured in the solid state and in acetonitrile solution. The transition energies and oscillator strengths were calculated with Time Dependent (TD) method to assign of charge transference (CT) electronic bands. The theoretical-experimental study of the vibrational and electronic properties confirms the structure proposed in this complex.

## 2. Experimental

### 2.1. General

Cobalt(II) nitrate, sodium diethyldithiocarbamate trihydrate salt and  $HNO_3$  were purchased from Vetec Co. All solvents and reagents were used as received without further purification. Elemental analysis (CHN) was carried out in a Sinc EA 1110 analyzer. The infrared spectra between 4000 and 370  $cm^{-1}$  were measured as a KBr pellet and polyethylene pellet at room temperature, on a Perkin Elmer 2000 FT-IR spectrometer. Data was collected with a resolution of 4  $cm^{-1}$ . Scanning speed 0.2  $cm^{-1} s^{-1}$  and 120 scans were used. The Raman spectra between 4000 and 100  $cm^{-1}$  were measured as a solid sample at room temperature, on a FT-Raman Bruker model RFS 100/S spectrometer. Data was collected with a resolution of 4  $cm^{-1}$  and 120 scans were used. Source setting: laser of 9394.75  $cm^{-1}$ ; 500 mW. Aperture setting: 7.0 mm. The solid state UV-Vis spectrum was acquired between 250 and 1000 nm, using a Varian Cary 5000 spectrophotometer. The UV-Vis spectrum in acetonitrile (MeCN) solution was acquired between 200 and 800 nm in a Varian Cary 50 spectrophotometer. The percentage of cobalt was determined by atomic absorption spectrometry using a Varian-1106 spectrophotometer. The  $pH_3O^+$  control during the synthesis of the complex was carried out with the potentiometer Micronal B 375.

### 2.2. Synthesis of bis-diethyldithiocarbamate Co (II)

To a solution of diethyldithiocarbamate (5 mmol) in 50 mL of deionized water was stirred by 20 min obtaining a  $pH_3O^+ = 10$ . The  $pH_3O^+$  was adjusted to 6.5 with  $HNO_3$  6 mol  $L^{-1}$ . Then cobalt(II) nitrate (0.914 g, 5 mmol) was added to this solution and the  $pH_3O^+$  was maintained around 6.5. This control was done using a potentiometer and all the synthesis was carried out under stirring at room temperature. The agitation was maintained for 10 min until the formation of a green solid precipitate. This precipitate was filtered under reduced pressure and washed for three times with deionized water.  $[Co(DDTC)_2]$  solid was kept under vacuum in a desiccator with sulfuric acid. Elemental analysis (CHN) and atomic absorption, for  $C_{10}H_{20}N_2S_4Co$  (Found C, 33.73%; N, 7.89%; H, 5.69% and Co, 16.20%. Calculated: C, 33.78%; N, 7.88%; and H, 5.67% and Co, 16.57%).

### 2.3. Calculations

The calculations were carried out for the neutral complex,  $[Co(DDTC)_2]$ , considered it as non-interacting independent units. The intermolecular interactions Metal-S and S-S were neglected in the present work and the results were compared with similar dithiolates [16,17]. The same approach, neglecting intermolecular interactions, was employed in a previous theoretical work on vibrational and UV-Vis spectroscopy of a series of anionic complexes of 1,3-dithiole-2-thione-4,5-dithiolate (dmit) and 1,3-dithiole-2-one-4,5-dithiolate (dmio), and a good agreement was obtained between calculated and experimental data [18,19].

For geometry optimization, the density functional theory methods (B3LYP and PBE1PBE) were used in the Gaussian 03 program [20]. For all calculations, we used the triple zeta 6-311G\*\* basis set in carbon, sulfur, nitrogen, hydrogen and cobalt atoms.

All calculations have been optimized from several initial geometries, in order to guarantee the global minima energy structures. After this procedure, the vibrational calculations were performed. No imaginary mode was observed. Characteristic normal stretching and bending modes from the  $-C_2H_5$  groups were visualized using the graphical Chemcraft program [21]. The skeletal or framework normal modes were determinate using the percentage deviation of the geometrical parameters (PDPG), from its equilibrium position. The study of the molecular orbitals was carried out using the Mulliken population analysis and a graphical analysis with the Chemcraft and GaussSum [22] programs. The information of the molecular orbitals was also evaluated through the density of states (DOS) spectra and orbital overlap population (OPDOS), using the GaussSum and QM-Forge [23] programs. Thus, the metal-sulfur interaction was described as bonding or antibonding.

The calculations of the transition energies and the oscillator strengths in the UV-Vis spectra of the optimized structures were carried out using the TD method, implemented in the Gaussian 03 with the transition moment calculation based on B3LYP and PBE1PBE orbitals. Evaluation of the theoretical methods was accomplished using the first 70 lowest energy states. The analysis of the TD/DFT states and the spectra simulation were carried out with the GaussSum program, using Gaussian functions with half-widths of 3500  $cm^{-1}$ . The incorporation of the solvent effect in the TD method, using the conductor polarizable calculation model (CPCM), was also carried out with MeCN.

Finally, to corroborate the previous observations, the analysis of the variation of the electronic density of this compound was carried out through Natural Orbital Bond (NBO). This method allowed us to qualitatively classify the main energy interactions among the atoms in the complex, according to the donation and retro-donation processes. The results were evaluated for both functional used in this study.

### 3. Results

#### 3.1. General

Monosodium DDTC salt is easily prepared by treatment of carbon disulfide with diethylamine in the presence of sodium hydroxide. This compound is a stable reagent in solid state, but the most important property of this ion is its protonation in acid solution

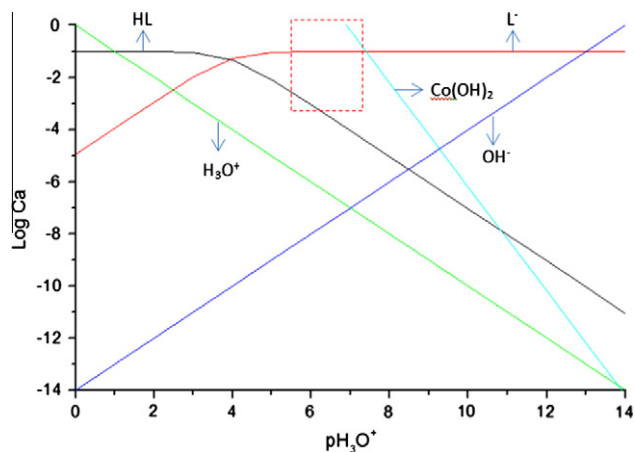


**Fig. 1.** Species distribution diagram of DDTC and of Co(OH)<sub>2</sub>. The detached region represents the great pH<sub>3</sub>O<sup>+</sup> of synthesis.

and subsequent decomposition into carbon disulfide and protonated amine. The composition is favoured when the pH<sub>3</sub>O<sup>+</sup> of the reactional mean is lower than pK<sub>a</sub> of the R<sup>+</sup>RNH<sub>2</sub><sup>+</sup> ion. The pK<sub>a</sub> of diethyldithiocarbamate acid derived from diethylamine is 3.95 in 19 °C [24]. Thus, the synthesis must be performed in optimum pH<sub>3</sub>O<sup>+</sup> range between 5.0 and 7.5. This prevents the decomposition of DDTC and the metal hydroxide formation.

The definition of these optimal conditions of synthesis was evaluated in different pH<sub>3</sub>O<sup>+</sup> conditions. These data were obtained from the graphical method [25], presented in Fig. 1. The graph shows the region of optimum pH<sub>3</sub>O<sup>+</sup> to perform the synthesis of the complex around 6.5. This allowed us to obtain the complex with an adequate yield and a purity satisfactory.

The solid obtained after purification was characterized through typical bands of the ligand in the infrared region, as νC–H stretchings between 3000 and 2900 cm<sup>-1</sup> and νC=N stretchings between 1500 and 1400 cm<sup>-1</sup>, presented in Fig. 2 for the IR and Raman spectra.

Also, UV–Vis experimental spectra are shown in Fig. 3. The solid state spectrum presents an appreciable enhancement of intensity in the region between 450 and 800 nm. This region was detached in the same figure, where we evidenced these transitions increasing by ten times the absorbance of the spectrum of [Co(DDTC)<sub>2</sub>], in solution of MeCN. Fig. 4 shows the deconvolution band analysis (DBA) of the UV–Vis spectra in the solid state and solution. In this figure is detached the UV–Vis spectrum of the [Co(DDTC)<sub>2</sub>] complex after further dilution with the purpose to demonstrate the CT bands lower to 250 nm.

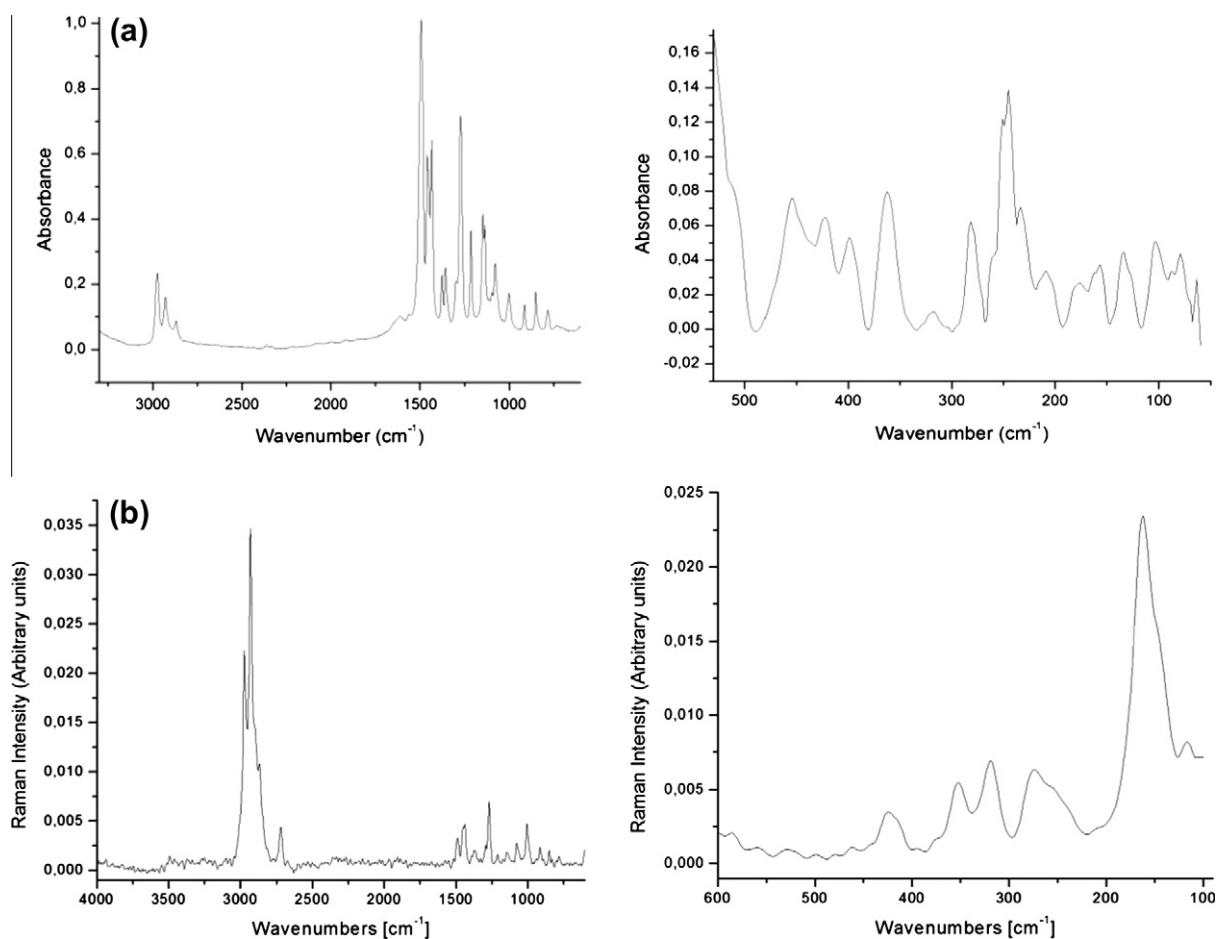


**Fig. 2.** Experimental spectra of [Co(DDTC)<sub>2</sub>]: (a) FT-IR spectra and (b) FT-Raman spectra.

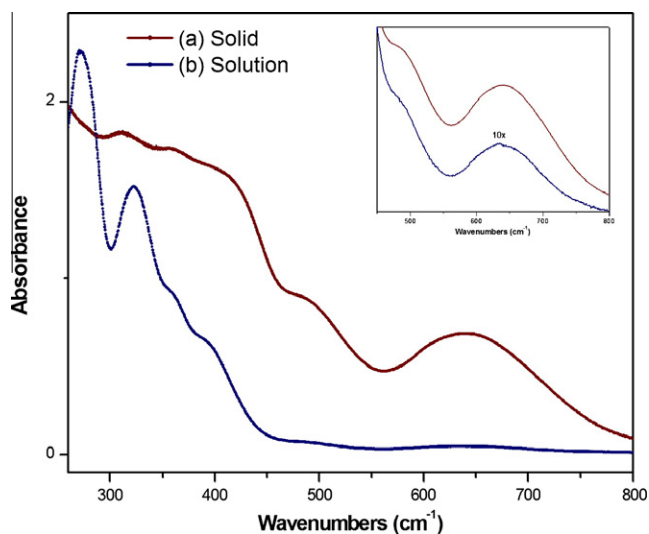


Fig. 3. UV-Vis spectra of [Co(DDTC)<sub>2</sub>]: (a) solid state; (b) acetronitrile solution.

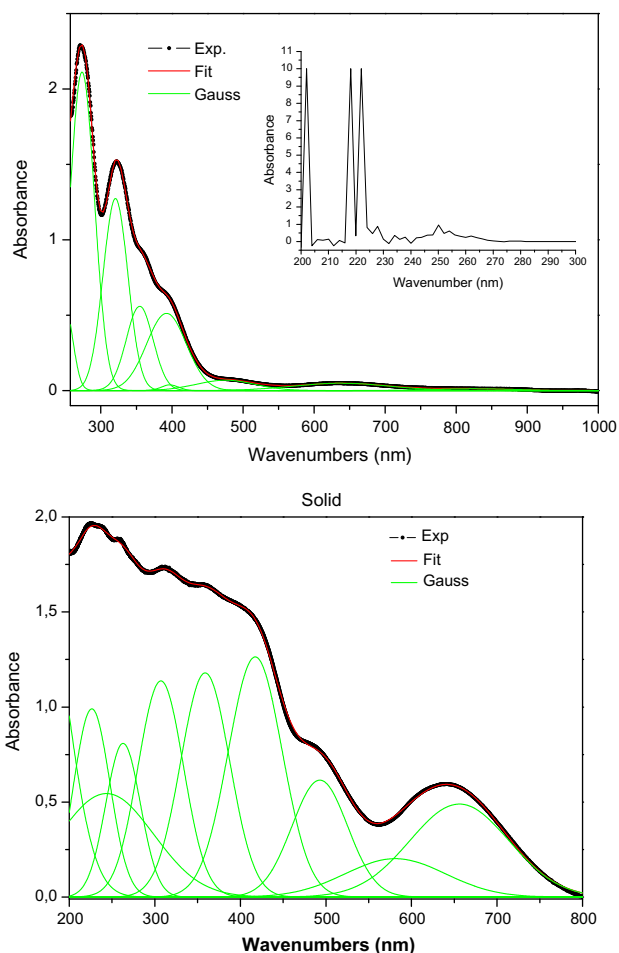


Fig. 4. Band deconvolution analysis of the UV-Vis spectra of [Co(DDTC)<sub>2</sub>].

A more detailed analysis of spectroscopic information of the complex was carried out through an theoretical-experimental assignment, considering structural parameters calculated by the proposal obtained by geometry optimization.

### 3.2. Optimization of the geometrical parameters

*Ab initio* optimization of the geometrical parameters, and the structural analysis of the [CoDDTC<sub>2</sub>] complex, was carried out employing the methods described above which are similar to the procedures found in the literature [26–30]. The B3LYP theoretical values for the Co–S, C=N and C–S bond lengths were of 2.29, 1.34 and 1.74 Å, without symmetry restrictions. The bond angles S(8)–Co–S(11) and S(9)–Co–S(10) were of 179.17° and 179.73°, respectively, showing a little deviation from the planar structure of the CoS<sub>4</sub> framework. Selected bond lengths and bond angles are given in Table 1. The complete structure of the [Co(DDTC)<sub>2</sub>] complex is represented in Fig. 5. Results were also evaluated with C<sub>2v</sub> symmetry for both methods (B3LYP and PBE1PBE) and are described in Table 1S of the Supplementary material. The values were similar to those observed with the calculations without symmetry, with fluctuations of less than two percent. These theoretical results were corroborated by crystallographic data of analogous dithiolates (iso-maleonitrile-dithiolate [16] and carbodiphosphorane CS<sub>2</sub> adduct [17]) coordinated with cobalt (III). In these dithiolates, the Co–S bonds observed are between 2.250 and 2.279 Å and the S–C bonds are between 1.689 and 1.717 Å. Another important structural parameter is the distance S–S that is responsible for the bite angle of the ligand to the metal. The theoretical calculations show an average value of 2.85 Å. This average value is higher than the values found in dithiolates, which were reported between 2.781 and 2.811 Å [16,17], as well as for S<sub>8</sub><sup>+</sup> cations which have S–S distances of 2.83 Å [31].

The charge distributions and bond order were also evaluated in this study. The results were obtained from the Mulliken population analysis and Mayer bond order. The results are described in Table 2S of the Supplementary material. The bond order for C–S and C=N confirm the electronic delocalization expected for this type of ligand with a planar characteristic. The values obtained for bond orders showed intermediate values between single and double bonds. The charge distributions within the complex was also important, especially the charge on the metal. According to Gorelsky et al. [32] for compounds [ML(SC<sub>6</sub>F<sub>5</sub>)] (M = first-row transition metal), the ionic contribution to the M–S bonds is related to the distribution of metal atomic charge and the thiolate ligand. For systems with a large metal charge, large ionic contributions and lower M–S bond orders are expected. The same tendency was found in the study of [M(L–L)<sub>2</sub>]<sup>–1</sup> (M=Sb or Bi; L–L = dmit or dmio) at RHF and DFT levels [33] and is also observed for the complex used in this work.

Table 1

Calculated parameters with B3LYP using 6-311G (d,p) and no symmetry for the [Co(DDTC)<sub>2</sub>] complex.

Atoms i, j	Bond lengths (Å)	Atoms i, j, k	Bond angles (°)	Atoms i, j, k	Bond angles (°)
R(1–8)	2.28	A(8–1–9)	78.33	A(2–3–4)	120.60
R(1–9)	2.29	A(8–1–10)	101.68	A(2–3–5)	120.91
R(1–10)	2.29	A(8–1–11)	179.17	A(8–2–9)	112.79
R(1–11)	2.28	A(1–8–2)	84.57	A(4–3–5)	118.48
R(2–3)	1.34	A(9–1–10)	179.73	A(10–12–11)	112.78
R(2–8)	1.73	A(9–1–11)	101.68	A(10–12–13)	123.42
R(2–9)	1.74	A(1–9–2)	84.29	A(11–12–13)	123.80
R(3–4)	1.47	A(10–1–11)	78.31	A(12–13–14)	120.61
R(3–5)	1.47	A(1–10–12)	84.30	A(12–13–15)	120.91
R(12–13)	1.34	A(1–11–12)	84.57	A(14–13–15)	118.48
R(13–14)	1.48	A(3–2–8)	123.79		
R(13–15)	1.47	A(3–2–9)	123.42		

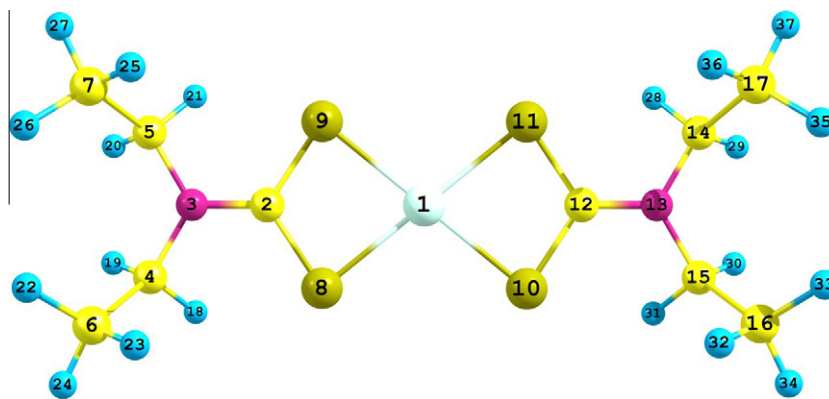


Fig. 5. DFT:B3LYP/6-311G (d,p) calculated structure for the  $[\text{Co}(\text{DDTC})_2]$  complex.

### 3.3. Vibrational assignments

Vibrational assignments were carried out with support of Density Functional Theory (DFT) calculations using the B3LYP method with a 6-311-G(d,p) basis set having the structural geometry obtained by the same method as the starting point. The calculated values with and without symmetry did not present imaginary frequencies and are described in Table 2. The simulated IR and Raman

spectra are found in Fig. 1S of the Supplementary material. For the discussion of the vibrational assignment, we took the DFT values corrected by the scale factor of 0.9613 as a base for comparison [34] in all fundamental vibrational modes,  $3n - 6 = 105$ . These adjusted data were associated with the second derivative spectrum and with DBA of the infrared bands of the  $[\text{Co}(\text{DDTC})_2]$  complex. For an accurate description of the normal modes in the metal-ligand spectral range, we use the percentage of deviation of the geo-

Table 2

Experimental FT-IR and FT-Raman and DFT-B3LYP/6-311G (d,p) calculated spectra for the  $[\text{Co}(\text{DDTC})_2]$  complex (wavenumber in  $\text{cm}^{-1}$ ).

$\text{Wn}_{\text{calc}}$ B3LYP ( $\text{C}_{2v}$ )	$I_{\text{IR}}^*$ ( $\text{C}_{2v}$ )	$I_{\text{R}}^{**}$ ( $\text{C}_{2v}$ )	$\text{Wn}_{\text{cor}}$ ( $\text{C}_{2v}$ )	Symm.	$\text{Wn}_{\text{calc}}$ B3LYP ( $\text{C}_1$ )	$I_{\text{IR}}^*$ ( $\text{C}_1$ )	$I_{\text{R}}^{**}$ ( $\text{C}_1$ )	$\text{Wn}_{\text{cor}}$ ( $\text{C}_1$ )	IR $\text{Wn}_{\text{Exp}}$ (%T)	IR DBA	Raman $\text{Wn}_{\text{Exp}}$	Raman DBA	Assignment (internal coordinate)
3127	0.09	20.68	3006	$a_1$	3128	23.51	16.31	3007					$\nu_{\text{as}}(\text{CH})(\text{CH}_3) + \nu_{\text{as}}(\text{CH})(\text{CH}_2)$
3127	102.29	17.99	3006	$b_2$	3128	76.95	16.27	3007					$\nu_{\text{as}}(\text{CH})(\text{CH}_3) + \nu_{\text{as}}(\text{CH})(\text{CH}_2)$
3123	0.00	0.54	3002	$a_2$	3124	3.71	2.89	3003					$\nu_{\text{as}}(\text{CH})(\text{CH}_3) + \nu_{\text{as}}(\text{CH})(\text{CH}_2)$
3123	5.42	5.26	3002	$b_1$	3123	3.07	2.41	3002			2990		$\nu_{\text{as}}(\text{CH})(\text{CH}_3) + \nu_{\text{as}}(\text{CH})(\text{CH}_2)$
3107	22.27	139.22	2987	$a_1$	3108	19.75	118.42	2988		2984			$\nu_{\text{s}}(\text{CH})(\text{CH}_3) + \nu_{\text{as}}(\text{CH})(\text{CH}_2)$
3107	7.98	1.11	2987	$b_2$	3108	9.67	19.37	2988					$\nu_{\text{s}}(\text{CH})(\text{CH}_3) + \nu_{\text{as}}(\text{CH})(\text{CH}_2)$
3104	68.56	0.93	2984	$b_1$	3105	46.20	58.07	2985		2979	2974	2975	$\nu_{\text{s}}(\text{CH})(\text{CH}_3) + \nu_{\text{as}}(\text{CH})(\text{CH}_2)$
3104	0.00	250.46	2984	$a_2$	3105	16.04	164.13	2985					$\nu_{\text{s}}(\text{CH})(\text{CH}_3) + \nu_{\text{as}}(\text{CH})(\text{CH}_2)$
3097	7.88	53.66	2977	$a_1$	3099	8.44	47.64	2979	2973 (60)	2971			$\nu_{\text{as}}(\text{CH})(\text{CH}_3) + \nu_{\text{as}}(\text{CH})(\text{CH}_2)$
3097	16.38	180.46	2977	$b_2$	3099	16.83	170.23	2979		2961			$\nu_{\text{as}}(\text{CH})(\text{CH}_3) + \nu_{\text{as}}(\text{CH})(\text{CH}_2)$
3092	0.00	68.84	2972	$a_2$	3093	2.64	72.49	2973					$\nu_{\text{as}}(\text{CH})(\text{CH}_3) + \nu_{\text{as}}(\text{CH})(\text{CH}_2)$
3092	11.10	50.02	2972	$b_1$	3093	11.15	54.77	2973	2953 (31)		2957	2956	$\nu_{\text{as}}(\text{CH})(\text{CH}_3) + \nu_{\text{as}}(\text{CH})(\text{CH}_2)$
3059	43.01	651.71	2941	$a_1$	3060	44.30	597.49	2942	2928 (84)	2930	2931	2932	$\nu_{\text{s}}(\text{CH})(\text{CH}_2)$
3059	66.61	74.36	2941	$b_2$	3060	63.44	105.25	2942		2913			$\nu_{\text{s}}(\text{CH})(\text{CH}_2)$
3053	0.00	0.62	2935	$a_2$	3054	0.77	4.93	2936			2907	2906	$\nu_{\text{as}}(\text{CH})(\text{CH}_2)$
3053	2.02	11.60	2935	$b_1$	3053	1.19	6.98	2935	2900	2902	2895		$\nu_{\text{as}}(\text{CH})(\text{CH}_2)$
3041	27.28	701.11	2923	$a_1$	3041	27.35	647.97	2923	2891	2883	2886		$\nu_{\text{s}}(\text{CH})(\text{CH}_3)$
3041	62.27	13.49	2923	$b_2$	3041	60.14	39.18	2923	2869	2867	2870	2868	$\nu_{\text{as}}(\text{CH})(\text{CH}_3)$
3038	18.97	0.02	2920	$b_1$	3039	13.43	30.41	2921		2862		2861	$\nu_{\text{as}}(\text{CH})(\text{CH}_3)$
3038	0.00	82.13	2920	$a_2$	3039	6.46	54.80	2921			2848	2847	$\nu_{\text{as}}(\text{CH})(\text{CH}_3)$
1533	13.96	52.44	1474	$a_1$	1533	18.62	50.31	1474	1505 (21)(sh)	1506		1500	$\nu_{\text{s}}(\text{C}=\text{N}) + \delta(\text{HCH})(\text{CH}_2)_{\text{sciss.}}$
1530	449.06	4.43	1471	$b_2$	1530	436.16	4.29	1471	1495 (12)	1497	1498	1497	$\nu_{\text{as}}(\text{C}=\text{N}) + \delta(\text{HCH})(\text{CH}_2)_{\text{sciss.}}$
1507	2.12	42.95	1449	$a_1$	1507	2.01	41.31	1449			1488	1489	$\delta(\text{HCH})(\text{CH}_3) + \nu_{\text{s}}(\text{C}=\text{N})$
1506	119.24	6.40	1448	$b_2$	1506	111.99	5.71	1448	1485 (18)	1486	1481	1483	$\delta(\text{HCH})(\text{CH}_3) + \nu_{\text{as}}(\text{C}=\text{N})$
1502	0.00	1.21	1444	$a_2$	1502	4.60	6.77	1444					$\delta(\text{HCH})(\text{CH}_3), (\text{CH}_2)$
1502	13.04	3.92	1444	$b_1$	1502	7.63	4.43	1444					$\delta(\text{HCH})(\text{CH}_3), (\text{CH}_2)$
1500	1.96	43.49	1442	$a_1$	1500	1.53	34.02	1442		1466			$\delta(\text{HCH})(\text{CH}_3), (\text{CH}_2)$
1500	0.00	9.23	1442	$b_2$	1500	1.56	13.58	1442	1458 (30)	1460			$\delta(\text{HCH})(\text{CH}_3), (\text{CH}_2)$
1490	0.00	5.31	1432	$a_2$	1490	0.07	5.04	1432	1451 (33)	1450	1452		$\delta(\text{HCH})(\text{CH}_3), (\text{CH}_2)$
1490	0.16	4.84	1432	$b_1$	1490	0.14	4.70	1432			1441	1447	$\delta(\text{HCH})(\text{CH}_3), (\text{CH}_2)$

(continued on next page)

Table 2 (continued)

Wn <sub>calc</sub> B3LYP (C <sub>2v</sub> )	I <sub>IR</sub> <sup>*</sup> (C <sub>2v</sub> )	I <sub>R</sub> <sup>**</sup> (C <sub>2v</sub> )	Wn <sub>cor</sub> (C <sub>2v</sub> )	Symm.	Wn <sub>calc</sub> B3LYP (C <sub>1</sub> )	I <sub>IR</sub> <sup>*</sup> (C <sub>1</sub> )	I <sub>R</sub> <sup>**</sup> (C <sub>1</sub> )	Wn <sub>cor</sub> (C <sub>1</sub> )	IR Wn <sub>Exp</sub> (%T)	IR DBA	Raman Wn <sub>Exp</sub>	Raman DBA	Assignment (internal coordinate)
1482	0.00	8.12	1425	a <sub>2</sub>	1482	0.69	9.14	1425	1434 (37)	1433	1436	1434	δ(HCH)(CH <sub>3</sub> ),(CH <sub>2</sub> )
1482	8.66	20.62	1425	b <sub>1</sub>	1482	8.85	20.14	1425		1406	1391	1383	δ(HCH)(CH <sub>3</sub> ),(CH <sub>2</sub> )
1473	15.82	20.96	1416	a <sub>1</sub>	1472	15.00	23.35	1415	1376 (71)	1378	1376		δ(HCH)(CH <sub>2</sub> ) + v <sub>s</sub> (C=N)
1471	435.54	21.02	1414	b <sub>2</sub>	1471	401.85	18.67	1414					δ(HCH)(CH <sub>2</sub> ) + v <sub>as</sub> (C=N)
1417	31.05	31.15	1362	a <sub>1</sub>	1417	30.55	29.83	1362		1371		1370	δ(HCH)(CH <sub>3</sub> ),(CH <sub>2</sub> )
1416	33.41	0.68	1361	b <sub>2</sub>	1416	33.41	1.08	1361	1359 (67)	1360	1363	1363	δ(HCH)(CH <sub>3</sub> ),(CH <sub>2</sub> )
1411	0.00	3.54	1356	a <sub>2</sub>	1410	6.31	2.24	1355	1353 (65)	1353			δ(HCH)(CH <sub>3</sub> ),(CH <sub>2</sub> )
1411	12.70	1.11	1356	b <sub>1</sub>	1410	6.55	2.26	1355	1341 (88)	1349	1345		δ(HCH)(CH <sub>3</sub> ),(CH <sub>2</sub> )
1400	0.60	4.53	1346	a <sub>1</sub>	1400	1.10	4.67	1346			1330		δ(HCH)(CH <sub>3</sub> ),(CH <sub>2</sub> ) + v <sub>s</sub> (C=N)
1399	161.31	1.18	1345	b <sub>2</sub>	1400	150.32	1.06	1346	1300 (88)	1300	1305		δ(HCH)(CH <sub>3</sub> ),(CH <sub>2</sub> ) + v <sub>as</sub> (C=N)
1383	0.00	3.51	1329	a <sub>2</sub>	1383	3.22	1.20	1329	1294 (75)	1293	1293	1294	δ(HCH)(CH <sub>3</sub> ),(CH <sub>2</sub> )
1383	5.41	0.00	1329	b <sub>1</sub>	1383	2.95	1.70	1329	1273 (13)	1277	1270	1271	δ(HCH)(CH <sub>3</sub> ),(CH <sub>2</sub> )
1341	44.32	0.22	1289	b <sub>1</sub>	1341	44.15	0.26	1289	1266 (27)	1268		1263	δ <sub>as</sub> (HCH)(CH <sub>3</sub> ),(CH <sub>2</sub> )
1341	0.00	21.05	1289	a <sub>2</sub>	1341	0.06	20.85	1289	1213 (52)	1213	1214	1218	δ <sub>as</sub> (HCH)(CH <sub>3</sub> ),(CH <sub>2</sub> )
1315	2.71	63.12	1264	a <sub>1</sub>	1315	2.77	63.22	1264					δ(HCH)(CH <sub>3</sub> ),(CH <sub>2</sub> ) + v <sub>s</sub> (C=N)
1311	422.69	2.41	1260	b <sub>2</sub>	1312	402.97	2.17	1261				1209	δ(HCH)(CH <sub>3</sub> ),(CH <sub>2</sub> ) + v <sub>as</sub> (C=N)
1236	91.37	0.19	1188	b <sub>1</sub>	1235	92.86	0.21	1187	1148 (46)	1149	1149	1199	δ(CNC) + δ(HCH)(CH <sub>3</sub> ),(CH <sub>2</sub> )
1234	0.00	3.96	1186	a <sub>2</sub>	1233	0.18	4.72	1185	1134 (10)	1135	1137	1173	δ(CNC) + δ(HCH)(CH <sub>3</sub> ),(CH <sub>2</sub> )
1174	1.35	8.18	1129	a <sub>1</sub>	1174	1.92	9.23	1129				1169	δ(HCH)(CH <sub>3</sub> ),(CH <sub>2</sub> ) + v <sub>s</sub> (C=N)
1173	142.16	0.81	1128	b <sub>2</sub>	1172	138.44	1.00	1127	1113 (17)	1114	1108	1152	δ(HCH)(CH <sub>3</sub> ),(CH <sub>2</sub> ) + v <sub>as</sub> (C=N)
1109	10.04	7.64	1066	a <sub>1</sub>	1110	11.55	6.68	1067					δ(HCH)(CH <sub>3</sub> ),(CH <sub>2</sub> )
1109	39.10	0.42	1066	b <sub>1</sub>	1109	47.97	0.64	1066	1098 (80)		1098		δ(HCH)(CH <sub>3</sub> ),(CH <sub>2</sub> )
1109	0.00	0.60	1066	a <sub>2</sub>	1108	18.35	0.78	1065				1085	δ(HCH)(CH <sub>3</sub> ),(CH <sub>2</sub> ) + v <sub>as</sub> (CN)
1109	60.54	0.10	1066	b <sub>2</sub>	1108	27.24	0.89	1065	1077 (63)	1075	1078	1077	δ(HCH)(CH <sub>3</sub> ),(CH <sub>2</sub> ) + v <sub>as</sub> (CN)
1084	15.64	0.00	1042	b <sub>1</sub>	1084	15.98	0.03	1042	1060 (80)		1065	1067	ρ(CH <sub>3</sub> )
1084	0.00	6.98	1042	a <sub>2</sub>	1083	0.01	6.78	1041			1060	1050	ρ(CH <sub>3</sub> )
1015	1.20	41.39	976	a <sub>1</sub>	1015	7.42	22.28	976	1014 (88)	1013	1005		v(CC) + v(CN) (N—CH <sub>2</sub> —CH <sub>3</sub> , ass. stretching)
1015	15.65	6.81	976	b <sub>2</sub>	1015	7.47	21.54	976	1001 (77)	999	990		v(CC) + v(CN) (N—CH <sub>2</sub> —CH <sub>3</sub> , ass. stretching)
1011	43.94	1.19	972	b <sub>1</sub>	1007	49.04	1.31	968	920 (18)	922		941	δ(NCS) <sub>s</sub> + δ(CCS) + v(CN)
1004	0.00	9.65	965	a <sub>2</sub>	997	0.02	14.22	958	914 (74)	914	915	914	δ(NCS) <sub>as</sub> + δ(CCS) + v(CN)
918	20.38	7.58	882	b <sub>1</sub>	918	23.92	7.45	882	912 (80)			889	ρ(CH <sub>3</sub> )
917	0.00	8.40	882	a <sub>2</sub>	915	0.00	12.47	880	880 (97)				ρ(CH <sub>3</sub> )
856	0.34	8.66	823	a <sub>1</sub>	855	0.29	5.71	822			850	851	ρ(CH <sub>3</sub> ) + ρ(CH <sub>2</sub> )
856	33.71	4.05	823	b <sub>2</sub>	855	37.14	4.20	822	847 (74)	844			ρ(CH <sub>3</sub> ) + ρ(CH <sub>2</sub> )
785	4.33	0.24	755	b <sub>1</sub>	785	3.58	0.69	755				829	ρ(CH <sub>3</sub> ) + ρ(CH <sub>2</sub> )
785	0.00	2.61	755	a <sub>2</sub>	784	0.82	2.22	754			804	803	ρ(CH <sub>3</sub> ) + ρ(CH <sub>2</sub> )
780	0.01	18.78	750	a <sub>1</sub>	780	0.08	16.64	750		791			ρ(CH <sub>3</sub> ) + ρ(CH <sub>2</sub> )
780	20.06	0.41	750	b <sub>2</sub>	779	17.96	0.47	749	785 (82)	785	785	782	δ(HCH)(CH <sub>3</sub> ) <sub>wagging</sub> + δ(HCH)(CH <sub>2</sub> ) <sub>twisting</sub>
611	1.78	5.92	587	a <sub>1</sub>	615	1.54	4.26	591	604 (89)		602	607	ρ(CH <sub>3</sub> ) + ρ(CH <sub>2</sub> )
610	3.50	0.12	586	b <sub>2</sub>	613	2.31	0.15	589	582 (70)		585	592	ρ(CH <sub>3</sub> ) + ρ(CH <sub>2</sub> )
567	0.00	16.26	545	a <sub>1</sub>	568	0.21	15.08	546	566 (71)			579	ρ(CH <sub>3</sub> ) + ρ(CH <sub>2</sub> )
565	10.69	0.09	543	b <sub>2</sub>	567	11.41	0.16	545	556 (73)		557	560	ρ(CH <sub>3</sub> ) + ρ(CH <sub>2</sub> )
469	14.54	0.29	451	b <sub>1</sub>	469	15.49	0.38	451	489 (74)				ρ(CH <sub>3</sub> ) + ρ(CH <sub>2</sub> )
468	0.00	0.00	450	a <sub>2</sub>	467	0.02	0.05	449					ρ(CH <sub>3</sub> ) + ρ(CH <sub>2</sub> )

Table 2 (continued)

Wn <sub>calc</sub> B3LYP (C <sub>2v</sub> )	I <sub>IR</sub> <sup>*</sup> (C <sub>2v</sub> )	I <sub>R</sub> <sup>**</sup> (C <sub>2v</sub> )	Wn <sub>cor</sub> (C <sub>2v</sub> )	Symm.	Wn <sub>calc</sub> B3LYP (C <sub>1</sub> )	I <sub>IR</sub> <sup>*</sup> (C <sub>1</sub> )	I <sub>R</sub> <sup>**</sup> (C <sub>1</sub> )	Wn <sub>cor</sub> (C <sub>1</sub> )	IR Wn <sub>Exp</sub> (%T)	IR DBA	Raman Wn <sub>Exp</sub>	Raman DBA	Assignment (internal coordinate)
445	4.81	8.95	428	a <sub>1</sub>	444	5.60	7.99	427	459 (73)		463		δ(SCS) <sub>s</sub>
442	1.04	0.02	425	b <sub>2</sub>	443	0.14	0.08	426	442 (73)		447		δ(SCS) <sub>as</sub>
432	1.37	3.39	415	a <sub>1</sub>	443	1.11	3.93	426	435 (73)		427	434	δ(CNC)
432	4.06	0.23	415	b <sub>2</sub>	432	1.84	1.46	415	419 (72)		416	421	δ(CNC)
373	136.22	0.03	359	b <sub>2</sub>	371	146.43	0.05	357	397 (69)	396			36.7% ν <sub>as</sub> (CoS) + 15.8% δ(SCS)
364	1.13	0.00	350	b <sub>1</sub>	353	1.61	0.02	339	361 (52)	361			51.3% ν <sub>as</sub> (CoS) + 14.4% δ(CoSC) + 8.9% δ(SCoS)
361	0.30	15.93	347	a <sub>1</sub>	345	0.20	22.70	332		354	352	352	23.4% ν <sub>s</sub> (CoS) + 27.9% δ(CoSC) + 19.7% δ(SCS) + 18.1% δ(SCN)
319	0.00	6.97	307	a <sub>2</sub>	315	0.01	6.93	303			320	319	28.7% ν <sub>s</sub> (CoS) + 17.4% δ(NCS) + 17.2% δ(SCN) + 8.7% δ(CoSC)
314	6.38	0.50	302	b <sub>1</sub>	313	7.00	0.52	301	303 (78)				25.2% δ(NCS) + 21.7% δ(SCoS) <sub>ang</sub> + 11.2% δ(SCoS) <sub>lin</sub>
308	0.68	0.01	296	b <sub>2</sub>	304	3.77	0.01	292	280 (68)	282			32.0% δ(CSCo) + 17.5% δ(SCoS) + 12.3% δ(SCS)
304	0.00	0.56	292	a <sub>2</sub>	302	0.01	1.83	290			276	276	31.2% ν <sub>s</sub> (CoS) + 28.2% δ(CoSC) + 19.5% δ(CNC)
267	0.07	0.00	257	b <sub>1</sub>	266	0.33	0.01	256	254 (80)	249	256	256	23.4% δ(SCN) + 22.4% δ(SCoS) <sub>ang</sub> + 11.5% δ(SCoS) <sub>lin</sub>
228	0.00	0.91	219	a <sub>1</sub>	228	0.00	0.57	219	224 (71)	224	242		τ(CH <sub>3</sub> )
228	0.00	0.32	219	a <sub>2</sub>	225	0.11	0.11	216					τ(CH <sub>3</sub> )
225	0.18	0.07	216	b <sub>2</sub>	223	0.01	0.40	214	202 (81)	204			τ(CH <sub>3</sub> )
192	0.11	0.03	185	b <sub>1</sub>	192	0.07	0.05	185					τ(CH <sub>3</sub> )
192	1.76	3.59	185	a <sub>1</sub>	185	2.22	1.29	178	178 (79)	176	177		37.7% δ(SCoS) <sub>lin</sub> + 16.7% δ(SCoS) <sub>ang</sub>
167	1.94	11.09	161	a <sub>1</sub>	161	1.15	5.65	155			163	163	τ(HCCH)(H <sub>3</sub> C—CH <sub>2</sub> —)
161	0.00	1.02	155	a <sub>2</sub>	158	1.06	2.43	152	130	142	145	150	τ(HCCH)(H <sub>3</sub> C—CH <sub>2</sub> —)
151	0.00	0.22	145	b <sub>2</sub>	151	0.00	0.19	145	118	119	118		τ(CCNC)(—CH <sub>3</sub> —CH <sub>2</sub> —N—CH <sub>2</sub> —)
134	1.40	3.51	129	a <sub>1</sub>	134	1.35	3.72	129	111	112			τ(CCNC)(—CH <sub>3</sub> —CH <sub>2</sub> —N—CH <sub>2</sub> —)
104	0.00	0.03	100	a <sub>2</sub>	95	0.26	0.24	91	105	106			τ(CCNC)(—CH <sub>3</sub> —CH <sub>2</sub> —N—CH <sub>2</sub> —)
95	0.22	0.15	91	b <sub>2</sub>	94	0.44	0.03	90	95	96			44.5% δ(SCoS) <sub>lin</sub>
86	1.30	1.92	83	b <sub>1</sub>	86	0.98	2.24	83		93			τ(CNCS)
85	0.19	4.07	82	a <sub>1</sub>	84	0.22	3.82	81	87	88			τ(CCNC)(CH <sub>3</sub> —CH <sub>2</sub> —N—CH <sub>2</sub> —)
60	2.77	1.49	58	b <sub>1</sub>	59	2.73	1.27	57		84			τ(CNCS)
45	0.00	0.00	43	b <sub>2</sub>	42	0.07	0.32	40	75	75			τ(CCNC)(CH <sub>3</sub> —CH <sub>2</sub> —N—CH <sub>2</sub> —)
44	0.00	0.25	42	a <sub>2</sub>	42	0.02	0.09	40					τ(CoSCN)
32	0.20	0.04	31	b <sub>1</sub>	33	0.25	0.05	32	66	64			τ(CNCC)
27	0.00	0.35	26	a <sub>2</sub>	28	0.01	0.24	27					τ(CNCC)
15	3.50	0.47	14	a <sub>1</sub>	14	3.46	0.34	13	54				τ(SCNC)

v: stretching mode, δ: bending mode, τ: torsion mode, ρ: rocking mode.

\* Calculated infrared intensities (I<sub>IR</sub>) are in Debye<sup>2</sup> Å<sup>-2</sup> amu<sup>-1</sup>.

\*\* Calculated Raman intensities (I<sub>R</sub>) are in Å<sup>4</sup> amu<sup>-1</sup>.

metrical parameters (PDGP) from the equilibrium position as described in others works [35–38]. The PDGP can also be normalized to obtain the percentage of participation of each internal vibrational coordinate that describes the framework vibrations, at all 26 coordinates (10 stretching and 16 bending). Assuming C<sub>2v</sub> symmetry for the [Co(DDTC)<sub>2</sub>] complex, the vibrational irreducible representation is Γ vibrational = 28a<sub>1</sub> + 25a<sub>2</sub> + 25b<sub>1</sub> + 27b<sub>2</sub>, where a<sub>2</sub> vibrational modes are not active in the infrared spectrum. Therefore 105 vibrational modes are expected in the Raman spectrum, from which 80 are infrared active (a<sub>1</sub>, b<sub>1</sub> and b<sub>2</sub>). The results with and without symmetry were compatible with the experimental data. The intensity variations between calculated and experimental FT-IR results are related with the nature of the experimental measure in the solid state and the calculations carried out in the vacuum, neglecting molecular interactions.

### 3.3.1. CH stretching

In the [Co(DDTC)<sub>2</sub>] complex, there are four —CH<sub>3</sub> groups and four —CH<sub>2</sub> groups totalizing 20 stretching ν(CH) vibrational modes.

In the FT-IR spectrum, Fig. 2a, we visualize in the region between 3000 and 2850 cm<sup>-1</sup> large bands with four peaks at 2973, 2928, 2900, 2869 cm<sup>-1</sup> and two shoulders at 2955 and 2895 cm<sup>-1</sup>. In the Raman spectrum, Fig. 2b, we visualize four well defined bands at 2974, 2931, 2870 and 2848 cm<sup>-1</sup>. We obtained the second derivative spectrum followed by DBA to achieve the maximum of observable bands. We emphasize eight fundamental bands by this procedure. Calculated and experimental wave numbers of the —CH stretching are given in Table 2.

### 3.3.2. C=N stretching

The C=N stretching bands were found in the FT-IR spectrum at 1505 and 1495 cm<sup>-1</sup> and by DBA at 1506 and 1497 cm<sup>-1</sup>. In the FT-Raman spectrum these bands were found at 1498 cm<sup>-1</sup> and by DBA at 1500 and 1497 cm<sup>-1</sup>. These bands were assigned with support of the calculated DFT vibrational spectrum. The comparison between calculated and experimental values for the ν(C=N) stretching was excellent, showing that these modes are coupled among different

internal coordinates. The scissoring  $\delta(\text{HCH})(\text{CH}_2)$  mode participates in the description of these normal mode.

### 3.3.3. HCH bending

In general terms, the HCH bending vibrations are considered as characteristic wavenumbers. In the infrared spectrum, Fig. 2a, we can observe in the region between 1497 and 1040  $\text{cm}^{-1}$ , 28 bands with support of DBA. In the Raman spectrum, Fig. 2b, we observe 26 bands with DBA support. These bands were assigned as HCH bending and are listed in Table 2. The rocking vibrations in both spectra were found in the region between 1060 and 785  $\text{cm}^{-1}$  with the DBA support, and the assignments are also presented in Table 2. A plot between bending and rocking experimental vibrations versus the calculated modes give the following results: correlation coefficients  $R = 0.9852$ , with  $\text{SD} = 22.24$  for the bending and  $R = 0.9926$ , with  $\text{SD} = 13.84$  for the rocking vibrations.

### 3.3.4. Skeletal framework vibrations

The identification of the metal-ligand vibrations was not straightforward as we have pointed out in other publications [35–38]. This is due to the higher mixture of the different internal coordinates that take part in the description of the normal modes. Thus, we studied the distorted geometry of each normal mode, observing the extension to which the equilibrium configuration parameters are dislocated. This procedure helps us to assign the low-energy bands.

In this approach, we used 10 stretching and 16 bending internal coordinates, which are inside of the skeletal framework of the complex in the description of the normal modes. The results presented below obey the following nomenclature: in bold characters we wrote (exp.IR) for experimental observation in the infrared spectrum, and (exp. R) for the Raman spectrum. The Deconvolution Band Analysis was written concisely as (DBA/IR; R). The abbreviation corr., means that the calculated wave number by the DFT:B3LYP/6-311G (d,p) procedure was scaled by 0.9613. The percentage (%) indicates the percentage variation of the bond lengths and bond angle.

- 359 corr. ( $b_2$ ), **397 (exp.IR), 396 (DBA/IR)**: 36.7%  $\nu_{\text{as}}(-\text{CoS}) + 15.8\% \delta(\text{SCS})$ .
- 350 corr. ( $b_1$ ), **361 (exp.IR), 364 (DBA/IR)**: 51.3%  $\nu_{\text{as}}(-\text{CoS}) + 14.4\% \delta(\text{CoSC}) + 8.9\% \delta(\text{SCoS})$ .
- 347 corr. ( $a_1$ ): **354 (DBA/IR), 352 (exp.R), 352 (DBA/R)**: 23.4%  $\nu_{\text{s}}(\text{CoS}) + 27.9\% \delta(\text{CoSC}) + 19.7\% \delta(\text{SCS}) + 18.1\% \delta(\text{SCN})$ .
- 307 corr. ( $a_2$ ): **320 (exp.R), 320 (DBA/R)**: 28.7%  $\nu_{\text{s}}(\text{CoS}) + 17.4\% \delta(\text{NCS}) + 17.2\% \delta(\text{SCN}) + 8.7\% \delta(\text{CoSC})$ .
- 302 corr. ( $b_1$ ), **303 (exp.IR)**: 25.2%  $\delta(\text{NCS}) + 21.7\% \delta(\text{SCoS})_{\text{ang}} + 11.2\% \delta(\text{SCoS})_{\text{lin}}$ .
- 296 corr. ( $b_2$ ), **280 (exp.IR), 282 (DBA/IR)**: 32.0%  $\delta(\text{CSCo}) + 17.5\% \delta(\text{SCoS}) + 12.3\% \delta(\text{SCS})$ .
- 292 corr. ( $a_2$ ): **276 (exp.R), 276 (DBA/R)**: 31.2%  $\nu_{\text{s}}(\text{CoS}) + 28.2\% \delta(\text{CoSC}) + 19.5\% \delta(\text{CNC})$ .
- 257 corr. ( $b_1$ ), **254 (exp.IR), 249 (DBA/IR), 256 (exp.R), 256 (DBA/R)**: 23.4%  $\delta(\text{SCN}) + 22.4\% \delta(\text{SCoS})_{\text{ang}} + 11.5\% \delta(\text{SCoS})_{\text{lin}}$ .
- 185 corr. ( $a_1$ ), **178 (exp.IR), 176 (DBA/IR), 177 (exp.R)**: 37.7%  $\delta(\text{SCoS})_{\text{linear}} + 16.7\% \delta(\text{SCoS})_{\text{Ang}}$ .
- 91 corr. ( $b_2$ ), **95 (exp.IR), 96 (DBA/IR)**: 44.5%  $\delta(\text{SCoS})_{\text{linear}}$ .

### 3.3.5. Torsional vibrations

The characterization of these torsional modes using the DFT results of the normal modes was rather complicated. To obtain an approximate assignment of these normal modes, we used the 3D computerized visualization. Eighteen torsional internal coordinates were defined in  $[\text{Co}(\text{DDTC})_2]$ . From the infrared spectrum we were able to associate 16 bands of weak intensity whose description are given in Table 2.

### 3.4. Molecular orbitals for $[\text{Co}(\text{DDTC})_2]$

The ground states of the complex show many occupied molecular orbitals, distributed between  $-5$  and  $-10$  eV in the vacuum. Table 3 presents the DFT orbitals, the Koopmans' energy and the Mulliken analysis of the occupied orbitals. Plots of the low energy occupied and virtual frontier orbitals in the ground state of  $[\text{Co}(\text{DDTC})_2]$  are presented in Fig. 6.

**Table 3**  
Koopmans' energy (eV), Mulliken population analysis and assignment for the frontier orbitals of  $[\text{Co}(\text{DDTC})_2]$ , with the B3LYP method.

Orbital	Symm.	Energy (eV)	B3LYP Alpha Mulliken population	Orbital	Symm.	Energy (eV)	B3LYP Beta Mulliken population
L + 11	$b_1$	1.86	$\sigma_{\text{C-H}}^+$ [Ethyl 93.1%]	L + 11	$a_2$	1.86	$\sigma_{\text{C-H}}^+$ [Ethyl 97.1%]
L + 10	$a_2$	1.85	$\sigma_{\text{C-H}}^+$ [Ethyl 97.7%]	L + 10	$a_1$	1.69	$\sigma_{\text{C-H}}^+$ [Ethyl 89.0%]
L + 9	$a_1$	1.68	$\sigma_{\text{C-H}}^+$ [Ethyl 89.7%]	L + 9	$b_2$	1.52	$\sigma_{\text{C-H}}^+$ [Ethyl 84.6%]
L + 8	$b_2$	1.52	$\sigma_{\text{C-H}}^+$ [Ethyl 85.0%]	L + 8	$a_1$	1.32	$\sigma_{\text{C-H}}^+$ + Co 4s [Co 56.3%; Ethyl 53.9%]
L + 7	$a_1$	1.30	$\sigma_{\text{C-H}}^+$ + Co 4s [Co 55.6%; Ethyl 54.8%]	L + 7	$b_1$	1.24	$\sigma_{\text{S-C}}^+$ [S 62.5%; C 18.7%; Ethyl 16.6%]
L + 6	$b_1$	1.25	$\sigma_{\text{S-C}}^+$ [S 62.3%; C 18.6%; Ethyl 16.9%]	L + 6	$a_1$	0.96	$\sigma_{\text{C-H}}^+$ + Co 4s [Ethyl 49.8%; Co 20.7%; S 19.7%]
L + 5	$a_1$	0.96	$\sigma_{\text{C-H}}^+$ + Co 4s [Ethyl 48.2%; Co 22.8%; S 18.8%]	L + 5	$b_2$	0.92	$\sigma_{\text{C-H}}^+$ [Ethyl 91.9%]
L + 4	$b_2$	0.92	$\sigma_{\text{C-H}}^+$ [Ethyl 91.9%]	L + 4	$a_1$	0.43	$\pi_{\text{S-Co}}^+$ [S 57.0%; Co 20.7%; Ethyl 23.1%]
L + 3	$a_1$	0.40	$\pi_{\text{S-Co}}^+$ [S 56.7%; Co 22.3%]	L + 3	$b_1$	-0.62	Co 3d [Co 94.0%]
L + 2	$b_2$	-0.73	$\pi_{\text{S-C=N}}^+$ [C 46.5%; S 30.9%]	L + 2	$b_2$	-0.72	$\pi_{\text{S-C=N}}^+$ [C 45.7%; S 31.6%]
L + 1	$a_1$	-1.19	$\pi_{\text{S-C=N}}^+$ [C 47.7%; S 29.3%]	L + 1	$a_2$	-0.80	Co 3d [Co 60.9%; S 36.7%]
LUMO	$a_2$	-1.58	Co 3d [Co 52.2%; S 45.9%]	LUMO	$a_1$	-1.20	$\pi_{\text{S-C=N}}^+$ [C 47.5%; S 29.6%]
HOMO	$b_2$	-5.57	Co 3d [Co 67.4%; S 15.2%]	HOMO	$b_2$	-4.96	Co 3d [Co 79.6%]
H-1	$a_1$	-5.88	Co 3d [Co 95.5%]	H-1	$a_1$	-5.21	Co 3d [Co 95.7%]
H-2	$b_1$	-5.96	$\pi_{\text{S}}^+$ [S 78.9%; Co 19.5%]	H-2	$a_2$	-6.12	$\pi_{\text{S}}^+$ [S 98.5%]
H-3	$a_2$	-6.16	$\pi_{\text{S}}^+$ [S 98.4%]	H-3	$b_1$	-6.42	$\pi_{\text{S}}^+$ [S 95.8%]
H-4	$b_1$	-6.37	$\pi_{\text{S}}^+$ [S 95.9%]	H-4	$b_1$	-6.59	$\pi_{\text{S}}^+$ [S 94.7%]
H-5	$a_1$	-7.02	$\pi_{\text{S}}^+$ [S 47.9%; N 36.4%]	H-5	$a_1$	-6.64	Co 3d [Co 94.6%]
H-6	$b_2$	-7.22	$\sigma_{\text{Co-S}}^+$ [S 54.5%; Co 16.1%; N 16.4%]	H-6	$a_1$	-7.01	$\pi_{\text{S}}^+$ [S 48.0%; N 36.4%; Ethyl 14.1%]
H-7	$a_1$	-7.24	Co 3d [Co 93.2%]	H-7	$b_2$	-7.12	$\sigma_{\text{Co-S}}^+$ [S 41.1%; N 29.7%; Co 14.5%]
H-8	$b_2$	-7.42	$\sigma_{\text{Co-S}}^+$ [S 61.0%; Co 13.6%; N 14.2%]	H-8	$a_2$	-7.38	$\sigma_{\text{Co-S}}^+$ [S 70.4%; Co 25.8%]
H-9	$a_2$	-7.70	$\sigma_{\text{Co-S}}^+$ [S 62.6%; Co 32.3%]	H-9	$b_2$	-7.43	$\sigma_{\text{Co-S}}^+$ [S 81.8%]
H-10	$b_1$	-8.17	Co 3d [Co 79.9%; S 19.8%]	H-10	$a_1$	-9.06	$\sigma_{\text{Co-S}}^+$ [S 72.0%; Co 17.9%]
H-11	$a_1$	-9.10	$\sigma_{\text{Co-S}}^+$ [S 68.9%; Co 20.7%]	H-11	$a_2$	-9.64	$\sigma_{\text{S-C}}^+$ [S 44.7%; C 22.3%; Ethyl 21.2%]

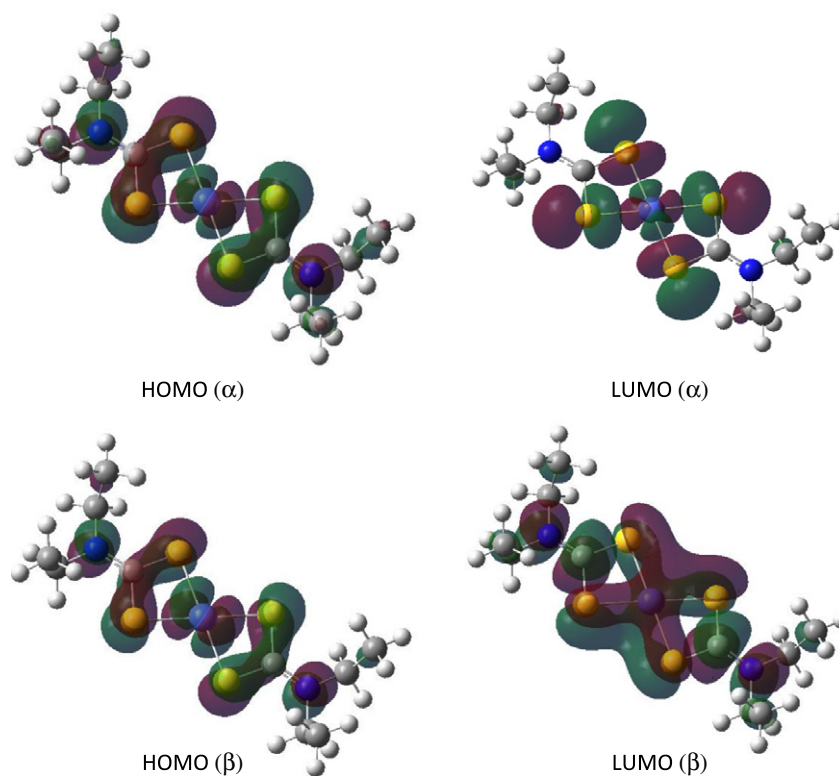


Fig. 6. Orbital representation of the HOMO ( $\alpha$ ), HOMO ( $\beta$ ), LUMO ( $\alpha$ ) and LUMO ( $\beta$ ), at PBE1PBE method of  $[\text{Co}(\text{DDTC})_2]$ . The contour values of the orbitals are all 0.02 a.u.

The Koopmans' energy difference between the highest occupied and the lowest unoccupied orbitals, HOMO( $\beta$ )–LUMO( $\alpha$ ) gap, was 3.38 eV for the B3LYP and 4.05 eV for the PBE1PBE. For both calculations, HOMO( $\beta$ ) orbital ( $b_2$  symmetry) was characterized by 3d metal ( $\sim 76\%$  to  $79\%$ ). The LUMO( $\alpha$ ) orbital ( $a_2$  symmetry) was characterized by 3d metal ( $\sim 52\%$ ) with the participation of the sulfur (46%) and could be interpreted as  $\sigma_{\text{Co-S}}$ . The orbital energies were similar in both methods. However, we see that the energy of the PBE1PBE orbitals is a few tenths higher than the B3LYP results. This is probably due to variations in methods and is also noticed for the HOMO–LUMO gap. Other orbitals are shown in Fig. 7. Also, the  $\pi_{\text{S-C=N}}^*$  and  $\pi_{\text{S}}$  orbitals are identified in the same order in this figure.

The participation of the metal orbitals were consistent with the evaluation of multiplicity adopts for  $d^7$  cobalt (II), duplet for one unpaired electron. This was confirmed by Mulliken atomic spin density analysis, which found a concentration of spin density on the metal, and compatible with the value of an unpaired electron. Fig. 2S describes the representation of the total spin density for B3LYP results, indicating low participation of spin density on the sulfur atoms of the DDTC ligand.

The analysis of the molecular orbitals obtained with the CPCM methodology, which incorporate the solvent effect, present some differences of HOMO–LUMO energy in both methods. However, the order of the frontier orbitals was not changed. This is clear by the analysis of the molecular orbital diagram obtained with the calculation carried out in MeCN, as displayed in Fig. 3S. The variation in the HOMO( $\beta$ )–LUMO( $\alpha$ ) gap with solvent, was of 3.28 and 3.97 eV for B3LYP and PBE1PBE, respectively.

From the final analysis obtained through the density of states, it is possible to rationalize the valence electronic structure of  $[\text{Co}(\text{DDTC})_2]$ . These results are shown in Table 3S and Fig. 8, where the degree of positive/negative overlap for frontier orbitals was detached in the OPDOS diagram. The frontier orbitals are populated by non-bonding orbitals, representing the isolated electron

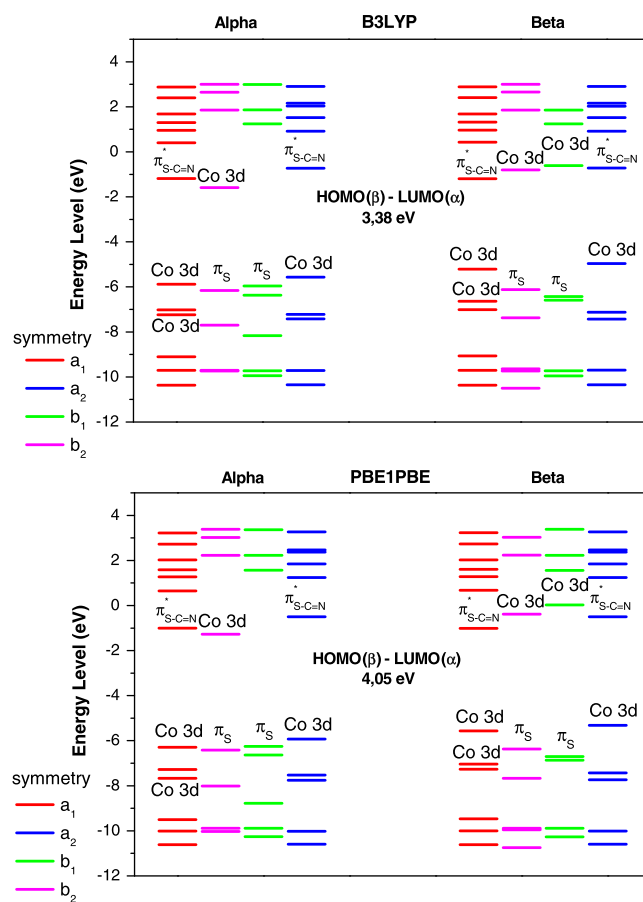
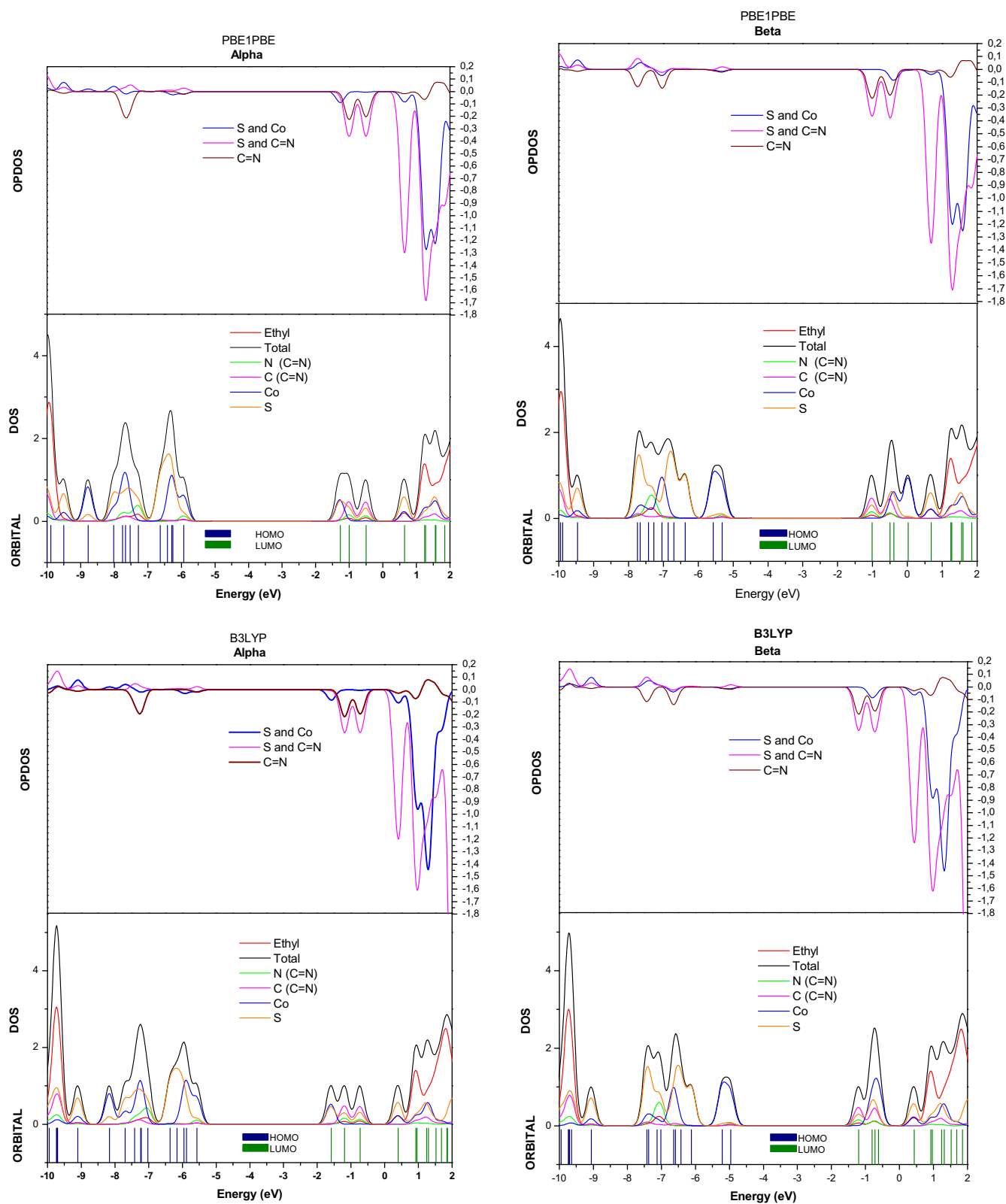


Fig. 7. Energy levels diagrams of  $[\text{Co}(\text{DDTC})_2]$ , with SCF molecular orbitals within the PBE1PBE and B3LYP methods.



**Fig. 8.** Molecular orbital diagram, density of states diagram (DOS) and orbital overlap population diagram (OPDOS) of the  $[\text{Co}(\text{DDTC})_2]$  complex, with the PBE1PBE and B3LYP methods.

of sulfur ( $\pi_s$ ) and d metal orbitals. The  $\pi_{\text{S-C=N}}^*$  orbitals are confirmed by the negative values and  $\sigma_{\text{Co-S}}$  are confirmed by the positive values. This analysis was important, especially to evaluate the nature of the electronic valence transitions.

### 3.5. Natural bond orbital analysis (NBO)

NBO analysis [39], at the B3LYP/6-311G (d,p) and PBE1PBE/6-311G (d,p) level were carried out to rationalize the factors contrib-

**Table 4**  
B3LYP/6-311G(d,p) donor–acceptor interactions between orbitals and stabilization energy (kcal/mol).

Donor orbital number	Description	Acceptor orbital number	Description	Stabilization energy (kcal/mol)
<i>Alpha electrons</i>				
1	BD (1)Co1–S8	451	BD*(1) C2–N3	5.51
2	BD (1)Co1–S9	451	BD*(1) C2–N3	5.51
88	LP (2) S8	452	BD*(2) C2–N3	25.22
90	LP (2) S9	452	BD*(2) C2–N3	25.22
449	BD*(1)Co1–S8	100	RY*(4)Co1	6.36
450	BD*(1)Co1–S9	100	RY*(7)Co1	6.36
89	LP (2) S10	450	BD*(1)Co1–S9	36.55
95	LP (3) S11	449	BD*(1)Co1–S8	36.54
89	LP (2) S10	472	BD*(1) C12–N13	6.00
91	LP (2) S11	469	BD*(1) S10–C12	30.75
92	LP (3) S11	472	BD*(1) C12–N13	6.00
93	LP (1) N13	469	BD*(1) S10–C12	54.24
<i>Beta electrons</i>				
1	BD (1)Co1–S8	451	BD*(1) C2–N3	5.67
2	BD (1)Co1–S9	451	BD*(1) C2–N3	5.67
22	BD (1) S8–S9	452	BD*(2) C2–N3	59.23
449	BD*(1)Co1–S8	99	RY*(6)Co1	5.60
450	BD*(1)Co1–S9	99	RY*(6)Co1	5.60
451	BD*(1) C2–N3	125	RY (1) C2	5.90
94	LP (2) S10	450	BD*(1)Co1–S9	34.64
96	LP (2) S11	449	BD*(1)Co1–S8	34.64
24	BD (1) S10–S11	472	BD*(2) C12–N13	59.23
94	LP (2) S10	471	BD*(1) C12–N13	6.12
96	LP (2) S11	471	BD*(1) C12–N13	6.12
471	BD*(1) C12–N13	271	RY*(1) C12	5.90

BD for 2-center bond, LP for 1-center valence lone pair, RY\* for 1-center Rydberg, and BD\* for 2-center antibond, the unstarred and starred labels corresponding to Lewis and non-Lewis NBOs, respectively.

**Table 5**  
PBE1PBE/6-311G(d,p) donor–acceptor interactions between orbitals and stabilization energy (kcal/mol).

Donor orbital number	Description	Acceptor orbital number	Description	Stabilization energy (kcal/mol)
<i>Alpha electrons</i>				
1	BD (1)Co1–S8	451	BD*(1) C2–N3	5.94
2	BD (1)Co1–S9	451	BD*(1) C2–N3	5.94
88	LP (2) S8	452	BD*(2) C2–N3	27.37
90	LP (2) S9	452	BD*(2) C2–N3	27.37
449	BD*(1) Co1–S8	86	LP*(7) Co1	5.49
449	BD*(1) Co1–S8	99	RY*(3) Co1	6.00
450	BD*(1) Co1–S9	86	RY*(3) Co1	5.49
450	BD*(1) Co1–S9	99	RY*(3) Co1	6.00
92	LP (2) S10	450	BD*(1)Co1–S9	39.77
95	LP (3) S11	449	BD*(1)Co1–S8	39.76
92	LP (2) S10	472	BD*(1) C12–N13	6.56
94	LP (2) S11	469	BD*(1) S10–C12	33.18
95	LP (2) S11	472	BD*(1) C12–N13	6.55
96	LP (1) N13	469	BD*(1) S10–C12	57.34
<i>Beta electrons</i>				
1	BD (1)Co1–S8	451	BD*(1) C2–N3	6.12
2	BD (1)Co1–S9	451	BD*(1) C12–N3	6.12
22	BD (1) S8–S9	452	BD*(2) C2–N3	65.13
451	BD (1) C2–N3	125	RY*(1) C2	7.12
86	LP (5) Co1	244	RY*(8) S10	5.17
86	LP (5) Co1	261	RY*(8) S11	5.17
24	BD (1) S10–S11	472	BD*(2) C12–N 13	65.13
94	LP (2) S10	450	BD*(1)Co1–S9	37.32
96	LP (2) S11	449	BD*(1)Co1–S8	37.32
94	LP (2) S10	471	BD*(1) C12–N13	6.69
96	LP (2) S11	471	BD*(1) C12–N13	6.69
471	BD*(1) C12–N13	271	RY*(1) C2	7.12

BD for 2-center bond, LP for 1-center valence lone pair, RY\* for 1-center Rydberg, and BD\* for 2-center antibond, the unstarred and starred labels corresponding to Lewis and non-Lewis NBOs, respectively.

uting to the total conformational energy. Using B3LYP/6-311G (d,p) procedure, for alpha electrons, the Co(1)–S(8) bond is formed by interaction between a  $sp^{0.03}d^{1.09}$  (47.12% s, 1.49% p and 51.38% d) orbital centered on the cobalt ion and a  $sp^{15.37}d^{0.02}$  (6.10% s,

93.75% p and 0.15% d) orbital on the sulfur atom; for beta electrons, the Co(1)–S(8) bond is formed by interaction between a  $sp^{0.03}d^{1.10}$  (46.74% s, 1.60% p and 51.65% d) orbital centered on the cobalt ion and a  $sp^{12.20}d^{0.02}$  (7.56% s, 92.29% p and 0.14% d) orbital on the sul-

**Table 6**  
Main singlet transition energies (eV) and the oscillator strength from the ground state of the [Co(DDTC)<sub>2</sub>] complex, with the PBE1PBE and B3LYP methods.

State	PBE1PBE			State	B3LYP		
	Dominant configuration*	Wavelength (nm)	Oscillator strength		Dominant configuration*	Wavelength (nm)	Oscillator strength
B <sub>1</sub>	HOMO(A) → LUMO(A) (35%) H-5(B) → L + 3(B) (59%)	1039	0.0000	B <sub>1</sub>	HOMO(A) → LUMO(A) (38%) H-5(B) → L + 3(B) (62%)	1047	0.0000
A <sub>2</sub>	H-7(A) → LUMO(A) (38%) H-5(B) → L + 2(B) (71%)	796	0.0000	A <sub>2</sub>	H-7(A) → LUMO(A) (26%) H-5(B) → L + 1(B) (64%)	745	0.0000
A <sub>2</sub>	H-7(A) → LUMO(A) (33%) H-2(A) → LUMO(A) (26%)	654	0.0000	A <sub>2</sub>	H-7(A) → LUMO(A) (43%) H-1(A) → LUMO(A) (21%)	647	0.0000
B <sub>1</sub>	H-5(B) → L + 3(B) (48%)	627	0.0000	B <sub>1</sub>	H-5(B) → L + 3(B) (48%)	629	0.0000
B <sub>2</sub>	H-10(A) → LUMO(A) (31%) H-1(A) → LUMO(A) (68%)	508	0.0001	B <sub>2</sub>	H-10(A) → LUMO(A) (25%) H-2(A) → LUMO(A) (74%)	535	0.0001
B <sub>2</sub>	HOMO(B) → LUMO(B) (91%)	415	0.0221	B <sub>2</sub>	HOMO(B) → LUMO(B) (94%)	452	0.0225
B <sub>2</sub>	HOMO(A) → L + 1(A) (79%)	337	0.0630	B <sub>2</sub>	HOMO(A) → L + 1(A) (85%)	364	0.0512
B <sub>2</sub>	H-4(A) → LUMO(A) (79%)	314	0.1622	B <sub>2</sub>	H-4(A) → LUMO(A) (77%) H-3(B) → L + 1(B) (20%)	337	0.1248
B <sub>1</sub>	H-1(A) → L + 1(A) (22%) H-3(B) → LUMO(B) (24%)	280	0.0156	B <sub>1</sub>	H-6(A) → LUMO(A) (19%) H-2(A) → L + 1(A) (22%) H-2(B) → L + 2(B) (17%)	294	0.0118
B <sub>1</sub>	H-6(A) → LUMO(A) (53%) H-3(A) → L + 2(A) (19%)	263	0.0174	B <sub>1</sub>	H-6(A) → LUMO(A) (57%) H-3(A) → L + 2(A) (19%)	280	0.0100
B <sub>2</sub>	H-3(B) → L + 2(B) (26%) H-2(B) → L + 3(B) (69%)	253	0.0235	B <sub>2</sub>	HOMO(A) → L + 3(A) (21%) H-5(B) → L + 2(B) (51%)	258	0.0280
B <sub>1</sub>	H-4(B) → LUMO(B) (55%)	246	0.0234	B <sub>1</sub>	H-3(A) → L + 2(A) (30%) H-9(B) → L + 1(B) (21%) H-2(B) → L + 2(B) (28%)	255	0.0491
B <sub>1</sub>	H-3(A) → L + 2(A) (27%) H-2(B) → L + 1(B) (38%)	241	0.0491	B <sub>2</sub>	H-3(B) → L + 1(B) (51%)	254	0.7403
B <sub>2</sub>	H-3(B) → L + 2(B) (44%) H-2(B) → L + 3(B) (15%)	237	0.7388	B <sub>2</sub>	HOMO(A) → L + 3(A) (18%) H-8(B) → L + 3(B) (28%) H-5(B) → L + 2(B) (29%)	252	0.0712
B <sub>2</sub>	H-8(A) → L + 1(A) (16%) H-6(A) → L + 1(A) (36%)	236	0.0744	B <sub>2</sub>	H-7(A) → L + 2(A) (31%) H-7(B) → LUMO(B) (20%)	227	0.1666
B <sub>2</sub>	H-6(A) → L + 1(A) (16%) H-8(B) → L + 3(B) (42%)	234	0.0610				
B <sub>1</sub>	H-7(B) → L + 2(B) (80%)	220	0.0139				
B <sub>2</sub>	H-8(A) → L + 1(A) (32%) H-9(B) → LUMO(B) (21%) H-7(B) → LUMO(B) (25%)	216	0.3227				
A <sub>1</sub>	HOMO(B) → L + 5(B) (77%)	215	0.0010				
B <sub>1</sub>	H-4(A) → L + 3(A) (43%) H-3(B) → L + 4(B) (31%)	214	0.0126				

A = alpha.

B = beta.

fur atom. The occupancy of the alpha and beta electrons in the Co(1)—S(8) bond was 1.93 electrons. The polarization coefficient for the formation of the bonding was 19.29% on the cobalt ion and 80.71% on the sulfur atom of the Co-S bond.

Using PBE1PBE/6-311G (d,p) procedure, for the alpha electrons, the Co(1)—S(8) bond was formed by interaction between a  $sp^{0.03}d^{1.09}$  (47.15% s, 1.64% p and 51.20% d) orbital centered on the cobalt ion and a  $sp^{14.52}d^{0.03}$  (6.43% s, 93.40% p and 0.16% d) orbital on the sulfur atom; for beta electrons, the Co(1)—S(8) bond was formed by interaction between a  $sp^{0.04}d^{1.10}$  (46.85% s, 1.76% p and 51.38% d) orbital centered on the cobalt ion and a  $sp^{11.54}d^{0.02}$  (7.96% s, 91.89% p and 0.15% d) orbital on the sulfur atom. The sum of the alpha and beta electrons occupancy was 1.93. The polarization coefficient for the formation of the bonding was 19.37% on the cobalt ion and 80.63% on the sulfur atom of the Co—S bond. In both cases, the results showed a higher polarization through the sulfur atom indicating a strong ionic character for the bond, and little difference in the hybrid bond description.

Results obtained by the methods DFT/B3LYP e DFT/PBE1PBE showed one bridge interaction with one electron of occupancy between the 3pz orbitals from the sulfur atoms of the diethyldithiocarbamate anion. The description of this interaction follows as procedure: NBO/B3LYP; S(8)—S(9) bridge with 0.70732 electrons occupancy giving an hybrid orbital  $s^0p^1d^0$  with 99.96% orbital p participation without appreciable polarization between the two sulfur atoms. The same results were found for the S(10)—S(11) interaction. In the PBE1PBE procedure, the occupancy was of 0.703736 electrons for the S(8)—S(9) and S(10)—S(11) interactions between the p orbitals. For C(2)=N(3) and C(12)=N(13) double bonds, the molecular orbital can be described as  $\sigma_{CN} = 0.6069(sp^{1.85})_C + 0.7948(sp^{1.68})_N$  and  $\pi_{CN} = 0.5181(sp^{99.99}d^{0.97})_C + 0.8553(sp^{99.99}d^{0.32})_N$ , with occupancy of 1.972 alpha electrons. For the beta electrons, the orbital wave function can be described as  $\sigma_{CN} = 0.6067(sp^{1.82})_C + 0.7949(sp^{1.68})_N$  and  $\pi_{CN} = 0.5175(sp^{99.99}d^{16.80})_C + 0.8557(sp^{99.99}d^{0.31})_N$ , with occupancy of 1.972 beta electrons. The polarization coefficients for the C and N atoms were of 31.83% for

**Table 7**Main singlet transition energies (eV) and the oscillator strength from the ground state of the [Co(DDTC)<sub>2</sub>] complex, with the PBE1PBE and B3LYP -CPCM methods.

State	PBE1PBE (MeCN)			B3LYP (MeCN)			
	Dominant configuration	Wavelength (nm)	Oscillator strength	State	Dominant configuration	Wavelength (nm)	Oscillator strength
B <sub>1</sub>	HOMO(A) → LUMO(A) (38%) H-4(B) → L + 3(B) (45%)	1098	0.0000	B <sub>1</sub>	HOMO(A) → LUMO(A) (41%) H-4(B) → L + 3(B) (49%)	1104	0.0000
A <sub>2</sub>	H-7(A) → LUMO(A) (32%) H-4(B) → L + 2(B) (63%)	858	0.0000	A <sub>2</sub>	H-1(A) → LUMO(A) (23%) H-4(B) → L + 1(B) (50%)	805	0.0000
A <sub>2</sub>	H-7(A) → LUMO(A) (39%) H-1(A) → LUMO(A) (20%)	713	0.0000	A <sub>2</sub>	H-7(A) → LUMO(A) (51%) H-4(B) → L + 1(B) (27%)	696	0.0000
B <sub>1</sub>	H-4(B) → L + 3(B) (63%)	631	0.0000	B <sub>1</sub>	H-4(B) → L + 3(B) (63%)	632	0.0000
B <sub>2</sub>	H-10(A) → LUMO(A) (33%) H-2(A) → LUMO(A) (66%)	518	0.0001	B <sub>2</sub>	H-10(A) → LUMO(A) (27%) H-2(A) → LUMO(A) (72%)	546	0.0001
B <sub>2</sub>	HOMO(B) → LUMO(B) (93%)	422	0.0471	B <sub>2</sub>	HOMO(B) → LUMO(B) (96%)	460	0.0487
B <sub>2</sub>	HOMO(A) → L + 1(A) (82%)	346	0.1718	A <sub>1</sub>	H-1(B) → LUMO(B) (100%)	429	0.0052
B <sub>1</sub>	H-3(A) → L + 2(A) (20%) H-2(A) → L + 1(A) (64%)	316	0.0236	B <sub>2</sub>	HOMO(A) → L + 1(A) (90%)	371	0.1362
B <sub>2</sub>	H-4(A) → LUMO(A) (94%)	313	0.2957	B <sub>2</sub>	H-4(A) → LUMO(A) (92%)	335	0.2552
B <sub>2</sub>	H-1(A) → L + 2(A) (54%)	285	0.0110	B <sub>1</sub>	H-2(A) → L + 1(A) (72%)	327	0.0272
B <sub>2</sub>	H-1(A) → L + 2(A) (26%) H-6(B) → L + 1(B) (11%) HOMO(B) → L + 4(B) (17%)	282	0.0125	B <sub>1</sub>	H-6(A) → LUMO(A) (38%)	290	0.0171
B <sub>1</sub>	H-6(A) → LUMO(A) (16%) H-2(A) → L + 1(A) (18%) H-5(B) → LUMO(B) (24%) H-2(B) → L + 1(B) (26%)	276	0.1195	B <sub>1</sub>	H-4(A) → L + 1(A) (40%) H-3(B) → LUMO(B) (38%)	289	0.0238
B <sub>1</sub>	H-6(A) → LUMO(A) (60%)	265	0.1173	B <sub>1</sub>	H-6(A) → LUMO(A) (32%) H-4(A) → L + 1(A) (25%)	284	0.0393
B <sub>1</sub>	H-8(A) → LUMO(A) (78%)	255	0.0922	B <sub>1</sub>	H-3(B) → LUMO(B) (35%)	281	0.0465
B <sub>2</sub>	H-3(B) → L + 2(B) (89%)	249	0.7362	B <sub>1</sub>	H-8(A) → LUMO(A) (72%)	270	0.0930
B <sub>1</sub>	H-3(A) → L + 2(A) (69%)	242	0.1704	B <sub>2</sub>	H-3(B) → L + 1(B) (59%) H-2(B) → L + 3(B) (37%)	270	0.2523
B <sub>2</sub>	H-5(B) → L + 2(B) (84%)	241	0.0389	B <sub>2</sub>	H-3(B) → L + 1(B) (26%) H-2(B) → L + 3(B) (56%)	264	0.5216
B <sub>2</sub>	H-2(B) → L + 3(B) (41%) HOMO(B) → L + 5(B) (42%)	236	0.1968	B <sub>2</sub>	HOMO(A) → L + 3(A) (86%)	263	0.0275
B <sub>2</sub>	H-2(B) → L + 3(B) (45%) HOMO(B) → L + 5(B) (45%)	236	0.1749	B <sub>2</sub>	H-5(B) → L + 1(B) (78%)	261	0.1655
B <sub>2</sub>	H-8(A) → L + 1(A) (33%) H-6(A) → L + 1(A) (37%)	234	0.0213	B <sub>1</sub>	H-3(A) → L + 2(A) (64%)	256	0.1860
B <sub>2</sub>	H-9(B) → LUMO(B) (35%) H-7(B) → LUMO(B) (23%)	231	0.0537	B <sub>2</sub>	H-8(A) → L + 1(A) (46%) H-6(A) → L + 1(A) (37%)	242	0.0782
B <sub>2</sub>	H-8(B) → L + 3(B) (78%)	227	0.0563	B <sub>1</sub>	H-7(B) → L + 1(B) (88%)	242	0.0392
B <sub>1</sub>	H-2(A) → L + 3(A) (30%) H-7(B) → L + 2(B) (54%)	225	0.0296	B <sub>2</sub>	H-9(B) → LUMO(B) (44%) H-7(B) → LUMO(B) (29%)	240	0.1442
B <sub>1</sub>	H-2(A) → L + 3(A) (55%) H-7(B) → L + 2(B) (32%)	224	0.0222	B <sub>2</sub>	H-8(A) → L + 1(A) (28%) H-9(B) → LUMO(B) (42%)	232	0.3728
B <sub>2</sub>	H-8(A) → L + 1(A) (27%) H-9(B) → LUMO(B) (42%)	223	0.3358	B <sub>1</sub>	H-9(B) → L + 1(B) (29%) H-6(B) → L + 3(B) (66%)	227	0.0728
B <sub>1</sub>	H-1(B) → L + 6(B) (95%)	220	0.0129				
B <sub>1</sub>	H-4(A) → L + 3(A) (27%) H-9(B) → L + 2(B) (41%) H-3(B) → L + 4(B) (19%)	213	0.2074				

A = alpha.

B = beta.

carbon and 68.17% for nitrogen. This shows a strong polarization directed toward the N atom. Similar results were found through the B3LYP procedure. For C(2)—S(8) bond, the molecular orbital can be described as  $\sigma_{CS} = 0.7494(sp^{2.09})_C + 0.6622(sp^{4.26})_S$ , with occupancy of 0.99147 for alpha electrons. For the beta electrons, the orbital wave function can be described as  $\sigma_{CS} = 0.7500(sp^{2.10})_C + 0.6614(sp^{4.15})_S$ , with occupancy of 0.99167 beta

electrons. The polarization coefficients for the C and S atoms were of 75.00% for carbon and 43.74% for sulfur. This shows a little polarization directed toward the C atom. Considering the similarity of the electronegativities in the C and S atoms, the slight polarization toward the carbon atom can be justified by the inductive effect produced by the vicinal C=N bond. Similar results were found through the PBE1PBE procedure.

### 3.5.1. Donor–acceptor interactions: Second Order Perturbation Theory Analysis of the Fox Matrix in NBO basis

A filled bonding or lone pair orbital can act as an electronic density donor. Conversely, an empty or filled bonding, anti-bonding orbital can act as an electronic density acceptor. The strength and weakness of bonds can be studied through these interactions. Tables 4 and 5 listed the donor and acceptor orbitals, electron occupancies and energy in kcal mol<sup>-1</sup>, higher than 5.0 kcal mol<sup>-1</sup>. The more representative interactions in the NBO/B3LYP calculations are between the orbitals: LP(1)N 13 to BD\*(1) S10–C12; LP (2) S10 to BD\*(1) Co1–S9; LP (3) S11 to BD\*(1) Co1–S8, with stabilization energy of 54.24, 36.55 and 36.54 kcal mol<sup>-1</sup> for alpha electrons, respectively. For beta electrons, the more representative interactions are between the orbitals BD (1) S8–S9 to BD\*(2) C2–N3; LP (2) S10 to BD\*(1) Co1–S9; BD (1) S10–S11 to BD\*(2) C12–N13, with stabilization energy of 59.23, 34.64, 34.64 and 59.23 kcal mol<sup>-1</sup>, respectively. For NBO/PBE1PBE, representative interactions were found between the orbitals: LP(2) S8 to BD\*(2) C2–N3; LP (2) S9 to BD\*(2) C2–N3; LP (2) S10 to BD\*(1) Co1–S9; LP (3) S11 to BD\*(1) Co1–S8; LP(2) S11 to BD\*(1) S10–C12 and LP (1) N13 to BD\*(1) S10–C12 with stabilization energy of 27.37, 27.37, 39.77, 39.77, 33.18 and 57.34 kcal mol<sup>-1</sup> for alpha electrons, respectively. For beta electrons, representative interactions are between the orbitals: BD (1) S8–S9 to BD\*(2) C2–N3; BD (1) S10–S11 to BD\*(2) C12–N13; LP (2) S10 to BD\*(1) Co1–S9; LP (2) S11 to BD\*(1) Co1–S8, with stabilization energy of 65.13, 65.13, 37.32 and 37.32 kcal mol<sup>-1</sup>, respectively.

### 3.6. Electronic UV–Visible spectra

Calculations of the transition energies and the oscillator strengths in the UV–Vis spectra of the optimized structures with C<sub>2v</sub> symmetry were realized with TD and TD-CPCM methods, using orbitals calculated with PBE1PBE and B3LYP. These calculations were carried out considering 70 singlet states and the results are presented in Fig. 4S and 5S as Supplemental material. Data from states with oscillator strengths greater than 0.01 a.u. are shown in a reduced form in Tables 6 and 7. The analysis of the states and the simulation of the spectra were carried out using the Chemcraft and GaussSum programs, and the obtained results are presented in Fig. 9. The first three calculated states were assigned as d → d transitions, with negative values indicating effect of spin contamination for those excited states due to triplet coupled single excitations. However, this did not interfere in the evaluation of other calculated states [40].

The literature doesn't have information about the charge transference spectrum for the bands in the [Co(DDTC)<sub>2</sub>] complex. However, for [Cu(DDTC)<sub>2</sub>], Cesur [41] proposes an analytic procedure for Cu(II) determination using displacement reactions of the metal cation Pb(II) in the complex [Pb(DDBC)<sub>2</sub>]. The effectiveness of the procedure was accompanied using UV–Vis spectroscopy, so the concentration of Cu(II) dissolved in chloroform was determined, but no assignment of the bands was done. San Andres et al. [42] reported a spectrophotometric determination of Cu(II), Ni(II) and Co(II) complexes with DDTC as ligand, but no assignment was done.

In [Co(DDTC)<sub>2</sub>], the calculated framework structure was square planar with Co(II) bound to four sulfur atoms. Co(II) is a d<sup>7</sup> system and had the possibility to achieve a low spin configuration. This was confirmed by analysis of molecular orbitals in the previous section. Urbach et al. [43] also discussed the circular dichroism spectra of low-spin square-planar schiff base cobalt (II) complexes. In this work, several additional transitions were observed and assigned as d → d transitions based on the energy and low intensity.

Other similar works with metal complex, using sulphurated ligands, was informed recently by Ferreira et al. [33,44]. In these studies, the complexes of zinc, antimony and bismuth with dmit

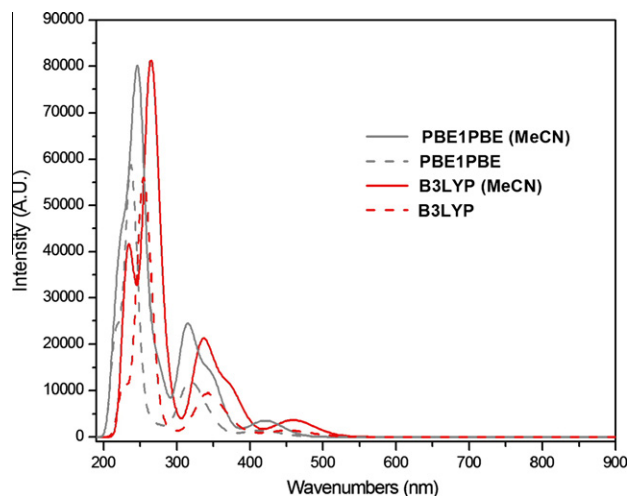


Fig. 9. UV–Vis TD-PBE1PBE, TD-B3LYP, TD-PBE1PBE–CPCM and TD-B3LYP–CPCM simulated spectra (190–900 nm) of [Co(DDTC)<sub>2</sub>], using the GaussSum program.

and dmio were studied by various singlet states with multi-configuration character using TD methods. This characteristic was also observed for the data obtained in [Co(DDTC)<sub>2</sub>] by the analysis of the coefficients of the dominant configuration.

Fig. 9 shows a comparison between the simulated data in solution and in vacuum. Also the two different DFT methods were compared and showed a delay of 19 nm. CPCM values were more realistic when compared to the intensity of the experimental data in the Fig. 3. The data obtained in the deconvolution of experimental spectra in Fig. 4, were used in comparison with theoretical data. Thus, the following discussion will be carried:

- The observed low-intensity bands at 656 and 581 nm in the solid state and 821 and 638 nm in MeCN solution were compared with the theoretical data in 858 and 713 nm for PBE1PBE and 805 and 696 nm for B3LYP. These states of A<sub>2</sub> symmetry were defined as d → d transitions with zero oscillator strengths, as expected for compounds with C<sub>2v</sub> symmetry. The intensity of these bands in the solid state is higher than the observed in solution, as we can see in Fig. 3. This can be explained by the existence of interactions in the solid state that allows the symmetry breaking.
- The observed low-intensity bands at 492 nm in solid state and 475 nm were compared with the theoretical data in 518 nm for PBE1PBE with d → d and 546 nm for B3LYP with π<sub>5</sub> → d. Again, the intensity of the band observed in the solid state was higher. Those observable are similar in shape and in intensity to the bands assigned for Urbach et al. [43], and in principle can be assigned as d → d transitions.
- The bands observed at 417 and 359 nm in the solid state and 397, 392 and 354 nm in solution were compared with the theoretical data in 422 and 346 nm for PBE1PBE and 460 and 371 nm for B3LYP. These states of oscillator strengths between 0.04 and 0.17 a.u. were classified as MLCT transitions.
- The band at 307 nm in solid state and 320 nm in solution was represented by state in 313 nm for PBE1PBE and 335 nm for B3LYP. The oscillator strength was calculated between 0.25 and 0.29 a.u. and was classified as LMCT transition.
- Finally, the other bands observed in the solid state between 262 and 226 nm and in solution between 276 and 213 nm were classified as LMCT and MLCT transitions. The values calculated for the oscillator strengths were between 0.2 and 0.7 a.u.

**Table 8**  
Electronic transitions assignment for the [Co(DDTC)<sub>2</sub>] complex.

Solid spectra (nm)	Solution spectra in MeCN (nm)	PBE1PBE (MeCN) (nm)	Assignment	B3LYP (MeCN) (nm)	Assignment
656/581	821/638	858/713	$\pi_S \rightarrow \pi_{S-C=N}^*$ $\sigma_{Co-S} \rightarrow \pi_{S-C=N}^*$	805/696	$\pi_S \rightarrow \pi_{S-C=N}^*$ Co 3d $\rightarrow$ Co 3d
492	475	518	Co 3d $\rightarrow$ Co 3d	546	$\pi_S \rightarrow$ Co 3d
417	397/392	422	Co 3d $\rightarrow \pi_{S-C=N}^*$	460	Co 3d $\rightarrow \pi_{S-C=N}^*$
359	354	346	Co 3d $\rightarrow \pi_{S-C=N}^*$	371	Co 3d $\rightarrow \pi_{S-C=N}^*$
307	320	313	$\pi_S \rightarrow$ Co 3d	335	$\pi_S \rightarrow$ Co 3d
262	276/274	276/265	Co 3d $\rightarrow \pi_{S-C=N}^*$ $\sigma_{Co-S} \rightarrow$ Co 3d	270/264	$\pi_S \rightarrow$ Co 3d $\pi_S \rightarrow$ Co 3d
243	250	249/242	$\pi_S \rightarrow$ Co 3d	256/240	$\pi_S \rightarrow$ Co 3d $\pi_S \rightarrow \pi_{S-C=N}^*$ $\sigma_{Co-S} \rightarrow \pi_{S-C=N}^*$
226	223	223	$\sigma_{Co-S} \rightarrow$ Co 3d	232	$\sigma_{Co-S} \rightarrow \pi_{S-C=N}^*$
	217	213	$\sigma_{Co-S} \rightarrow \pi_{S-C=N}^*$	227	Co 3d $\rightarrow \pi_{S-C=N}^*$

Final electronic transitions assignments in the UV–Vis spectra, based on the experimental data and theoretical results, are summarized in Table 8.

#### 4. Conclusions

Synthesis, elementary CHN analysis, UV–Vis, and infrared spectrum of the [Co(DDTC)<sub>2</sub>] complex were presented. Theoretical calculations concerning structural analysis show a pseudo planar framework structure for the CoS<sub>4</sub> chromosphere. Vibrational assignments of bands in the infrared spectrum of the [Co(DDTC)<sub>2</sub>] complex have been done based on the DFT: B3LYP/6-311G(d,p) quantum mechanical calculation. The most probable assignment for the skeletal vibrations was based on the interpretation of the distorted geometry of the normal modes, having as focus the study of the percentage of deviation of the geometrical parameters. The results suggest the structure depicted in Fig. 6 as the most probable, and the full assignment for the complex is presented in Table 2. The NBO results using B3LYP/6-311G (d,p) procedure, for alpha electrons, indicates that the Co(1)–S(8) bond is formed by interaction between a  $spd^{0.03}d^{1.09}$  (47.12% s, 1.49% p and 51.38% d) orbital centered on the cobalt ion and a  $sp^{15.37}d^{0.02}$  (6.10% s, 93.75% p and 0.15% d) orbital on the sulfur atom; for beta electrons, the Co(1)–S(8) bond is formed by interaction between a  $spd^{0.03}d^{1.10}$  (46.74% s, 1.60% p and 51.65% d) orbital centered on the cobalt ion and a  $sp^{12.20}d^{0.02}$  (7.56% s, 92.29% p and 0.14% d) orbital on the sulfur atom. The occupancy of the alpha and beta electrons in the Co(1)–S(8) bond was of 1.93 electrons. Similar results were found for the PBE1PBE/6-311G (d,p). The NBO results also indicate an interaction between S–S atoms in each diethyldithiocarbamate ligands. The donor–acceptor interactions based on the Second Order Perturbation Theory Analysis of the Fox Matrix were also carried out.

The UV–Vis spectra of the [Co(DDTC)<sub>2</sub>] complex were measured in the solid state and in acetonitrile solution. The multi-configurational nature of several excited states of complex involving intra-ligand transitions are also observed. The calculated results are in agreement with the experimental spectra, confirming the existence of several LMCT and MLCT transitions. Analyses of the transition energies, using the TD-B3LYP and TD-PBE1PBE methods, are in excellent agreement with the experimental results. The CI calculations allowed a more precise analysis than the previous one obtained from simple analysis of the boundary orbitals. The calculations, carried out with solvent effect, described the energies with a larger precision than in the vacuum system, although the intensity was not properly represented.

#### Acknowledgments

We are grateful to the Brazilian agencies CNPq, FAPERJ, FAPESP for financial support, and to CAPES (PNPD). Thanks are given to the Consejo Superior de Investigaciones Científicas (CSIC) of Spain for the award of a license for the use of the Cambridge Crystallographic Data Base (CSD). We thank Prof<sup>a</sup>. Dr. Nadia M. Comerlato and Prof<sup>a</sup>. Dr. Cássia C. Turci for their valuable suggestions about the text.

#### Appendix A. Supplementary material

The UV–Vis theoretical results of [Co(DDTC)<sub>2</sub>] and the infrared band deconvolution analysis are available as Supplementary data associated with this article can be found, in the online version, at <http://dx.doi.org/10.1016/j.molstruc.2012.06.041>.

#### References

- [1] J.M. Yuhas, F. Culo, Cancer Treat. Rep. 64 (1980) 57.
- [2] S.B. Howell, R. Taetle, Cancer Treat. Rep. 64 (1980) 611.
- [3] K. Lemma, S.K.C. Elmroth, L.I. Elding, J. Chem. Soc., Dalton Trans. (2002) 1281–1286.
- [4] Z. Rehman, N. Muhammad, S. Ali, I.S. Butler, A. Meetsma, Inorg. Chim. Acta 376 (2011) 381–388.
- [5] G. Faraglia, S. Sitran, D. Montagner, Inorg. Chim. Acta 358 (2005) 971–980.
- [6] N. Singh, S. Bhattacharya, J. Organomet. Chem. 700 (2012) 69–77.
- [7] J.M. Berry, C. Jacobs, B. Sikic, J. Halsey, R.F. Borch, J. Clin. Oncol. 8 (1990) 1585–1590.
- [8] Y.C. Zhang, G.Y. Wang, X.Y. Hu, Q.F. Shi, T. Qiao, Y. Yang, J. Cryst. Growth 284 (3/4) (2005) 554–560.
- [9] T.K. Jana, D.P. Kumar, R. Pradhan, S. Dinda, P.N. Ghosh, C. Simmonet, J. Marrot, I. Imaz, A. Wattiaux, J.-P. Sutter, F. Secheresse, R. Bhattacharyya, Inorg. Chim. Acta 362 (10) (2009) 3583–3594.
- [10] I.M. Oglezneva, L.N. Mazalov, J. Struct. Chem. 43 (2) (2002) 352–354.
- [11] G. Bauer, G.S. Nikolov, N. Trendafilova, J. Mol. Struct. 415 (1997) 123–134.
- [12] H.P.S. Chauhan, N.M. Shaik, J. Inorg. Biochem. 99 (2) (2005) 538–545.
- [13] I. Georgieva, N. Trendafilova, J. Phys. Chem. A 111 (50) (2007) 13075–13087.
- [14] M.P. San Andres, M.L. Marina, S. Vera, Talanta 41 (2) (1994) 179–185.
- [15] H. Mikosch, G. Bauer, R. Kellner, N. Trendafilova, G. Nikolov, J. Mol. Struct. 142 (1986) 473–476.
- [16] B.S. Kang, Z.N. Chen, Z. Lin, H.X. Zhang, H.Q. Liu, X.Y. Huang, J. Coord. Chem. 46 (1999) 409.
- [17] W. Petz, B. Neumuller, J. Hehl, Z. Anorg. Allg. Chem. 632 (2006) 2232.
- [18] G.B. Ferreira, N.M. Comerlato, J.L. Wardell, E. Hollauer, J. Braz. Chem. Soc. 15 (2004) 951–963.
- [19] G.B. Ferreira, N.M. Comerlato, J.L. Wardell, E. Hollauer, Spectrochim. Acta Part A 61 (2005) 2663–2676.
- [20] Gaussian 03, Revision C.02, M.J. Frisch, G.W. Trucks, H.B. Schlegel, G.E. Scuseria, M.A. Robb, J.R. Cheeseman, J.A. Montgomery, Jr., T. Vreven, K.N. Kudin, J.C. Burant, J.M. Millam, S.S. Iyengar, J. Tomasi, V. Barone, B. Mennucci, M. Cossi, G. Scalmani, N. Rega, G.A. Petersson, H. Nakatsuji, M. Hada, M. Ehara, K. Toyota, R. Fukuda, J. Hasegawa, M. Ishida, T. Nakajima, Y. Honda, O. Kitao, H. Nakai, M. Klene, X. Li, J.E. Knox, H.P. Hratchian, J.B. Cross, V. Bakken, C. Adamo, J. Jaramillo, R. Gomperts, R.E. Stratmann, O. Yazyev, A.J. Austin, R. Cammi, C.

- Pomelli, J.W. Ochterski, P.Y. Ayala, K. Morokuma, G.A. Voth, P. Salvador, J.J. Dannenberg, V.G. Zakrzewski, S. Dapprich, A.D. Daniels, M.C. Strain, O. Farkas, D.K. Malick, A.D. Rabuck, K. Raghavachari, J.B. Foresman, J.V. Ortiz, Q. Cui, A.G. Baboul, S. Clifford, J. Cioslowski, B.B. Stefanov, G. Liu, A. Liashenko, P. Piskorz, I. Komaromi, R.L. Martin, D.J. Fox, T. Keith, M.A. Al-Laham, C.Y. Peng, A. Nanayakkara, M. Challacombe, P.M.W. Gill, B. Johnson, W. Chen, M.W. Wong, C. Gonzalez, J.A. Pople, Gaussian, Inc., Wallingford, CT, 2004.
- [21] Chemcraft Software. <<http://www.chemkraftprog.com/order.html>>.
- [22] N.M. O'Boyle, A.L. Tenderholt, K.M. Langner, J. Comp. Chem. 29 (2008) 839–845.
- [23] Tenderholt, Adam L. QMForge, Version 2.1. <<http://qmforge.sourceforge.net>>.
- [24] R. Zahradnik, P. Zuman, Chem. Commun. 24 (1959) 1132.
- [25] H. Freiser, Q. Fernando, Ionic Equilibria in Analytical Chemistry, John Wiley & Sons, Inc., New York, 1963.
- [26] J.M. Ramos, R.M. Viana, C.A. Téllez Soto, W.C. Pereira, A.O. Izolani, M.I.P. Silva, Spectrochim. Acta A 65 (2006) 433–438.
- [27] C.A. Téllez Soto, J.M. Ramos, R.S. Rianelli, M.C.B.V. Souza, V.F. Ferreira, Spectrochim. Acta A 67 (2007) 1080–1087.
- [28] J.M. Ramos, O. Versiane, C.A. Téllez Soto, Spectrochim. Acta A 67 (2007) 1046–1054.
- [29] O. Versiane, B.L. Rodrigues, J.M. Ramos, C.A. Téllez Soto, Spectrochim. Acta A 65 (2006) 1112–1119.
- [30] J.M. Ramos, G.F. Ondar, O. Versiane, C.A. Téllez Soto, Spectrochim. Acta A 71 (2008) 1364–1370.
- [31] D.F. Shriver, P.W. Atkins, Inorganic Chemistry, fourth ed., Oxford University Press, New York, 2006.
- [32] S.I. Gorelsky, L.B. Basumallick, J. Vura-Weis, R. Sarangi, K.O. Hodgson, B. Hedman, K. Fujisawa, E.I. Solomon, Inorg. Chem. 44 (2005) 4947.
- [33] G.B. Ferreira, E. Hollauer, N.M. Comerlato, J.L. Wardell, Spectrochim. Acta Part A 71 (2008) 215–229.
- [34] L. Radom, A.P. Scott, J. Phys. Chem. 100 (1996) 16502.
- [35] B.A. Almeida, J.M. Ramos, O. Versiane, M. Souza, C.A. Téllez Soto, A.L.R. Mercê, A.S. Mangrich, Polyhedron 27 (2008) 3662–3668.
- [36] J.M. Ramos, M.T.M. Cruz, A.C. Costa Jr., O. Versiane, C.A. Téllez Soto, ScienceAsia 37 (2011) 247–255.
- [37] J.M. Ramos, O. Versiane, C.A. Téllez Soto, Spectrochim. Acta A 68 (2007) 1370–1378.
- [38] J.M. Ramos, O. Versiane, C.A. Téllez Soto, Spectrochim. Acta A 72 (2009) 182–189.
- [39] F. Weinhold, C. Landis, Valency and Bonding: A natural Bond Orbital Donor–Acceptor Perspective, Cambridge University Press, 2005.
- [40] Z. Li, W. Liu, J. Chem. Phys. 135 (2011) 194106.
- [41] H. Cesur, Chem. Pap. 61 (2007) 342–347.
- [42] M.P. San Andres, M.L. Marina, S. Vera, Analyst 120 (1995) 255.
- [43] F.L. Urbach, R.D. Bereman, J.A. Topich, M. Hariharan, B.J. Kalbacher, J. Am. Chem. Soc. 96 (16) (1974) 5063–5069.
- [44] G.B. Ferreira, E. Hollauer, N.M. Comerlato, J.L. Wardell, Inorg. Chim. Acta 359 (2006) 1239–1247.